CZECH UNIVERSITY OF LIFE SCIENCES
PRAGUE
FACULTY OF ENVIRONMENTAL SCIENCE

MASTER THESIS

2015 Jiří Roubínek

CZECH UNIVERSITY OF LIFE SCIENCES PRAGUE
FACULTY OF ENVIRONMENTAL SCIENCE
Department of Water Resources and Environmental Modeling
and
WSL Institute for Snow and Avalanche Research SLF

LINKING SNOW DISTRIBUTION AND FOREST CANOPY CHARACTERISTICS BY WAY OF HEMISPHERICAL PHOTOGRAPHY

MASTER THESIS

Supervisor - CULS: Ing. Jiří Pavlásek Ph.D.
Supervisors – SLF: Dr. Tobias Jonas; MSc. David Moeser
Author: Bc. Jiří Roubínek

2015

WSL Institute for Snow and Avalanche Research SLF
CZECH UNIVERSITY OF LIFE SCIENCES PRAGUE

CZECH UNIVERSITY OF LIFE SCIENCES PRAGUE

Faculty of Environmental Sciences

DIPLOMA THESIS ASSIGNMENT

Bc. Jiří Roubínek

Environmental Modelling

Thesis title

Linking snow distribution and forest canopy characteristics by way of hemispherical photography

---

Objectives of thesis

Main aim of this study is to investigate the temporal and spatial dynamics between the forest canopy and the underlying snow pack.

Three main goals are defined:
1) Study the snow cover in forested sites and its relation to canopy.
2) Study the canopy at these sites. Compare several methods.
3) Quantify the snow-canopy relation and propose snow model.

Methodology

A series of field areas under various canopy and elevation classes centered around Davos, Switzerland containing approximately 2000 geo-rectified (+/-50cm) and labeled points will be setup to allow for repeatable measurements of total snow depth, new snow depth and snow depletion rates. Canopy coverage characteristics will be estimated by a variety of methods, (1) hemispherical photography, (2) manual characterization and (3) airborne light detection and ranging data.

The canopy characteristics derived from these methods will be analyzed for correlation to manual snow measurements collected at the field sites. These methods will be then compared and evaluated for applicability to large scale forest snow studies.

The proposed extent of the thesis

50 pages

Keywords

snow hydrolog, light detection and ranging (LiDAR), leaf area index (LAI)

Recommended information sources

Essery, R., Rutter, N., Pomeroy, J., Baxter, R., Stähli, M., Gustafsson, D., Barr, A., Bartlett, P., Elder, K., 2009. SNOWMIP2: An Evaluation of Forest Snow Process Simulations. Bull. Am. Meteorol. Soc. 90, 1120–1135. doi:10.1175/2009BAMS2629.1

Gelfan, A.N., Pomeroy, J.W., Kuchment, L.S., 2004. Modeling Forest Cover Influences on Snow Accumulation, Sublimation, and Melt. J. Hydrometeorol. 5, 785–803. doi:10.1175/1525-7541(2004)005<0785:MFCIOS>2.0.CO;2

Gray, D.M., Male, D.H., 2004. Handbook of Snow: Principles, Processes, Management & Use. Blackburn Press.

Chianucci, F., Cutini, A., 2012. Digital hemispherical photography for estimating forest canopy properties: current controversies and opportunities. iForest – Biogeosciences For. 290–295. doi:10.3832/ifor0775-005

Jonas, T., Marty, C., Magnusson, J., 2009. Estimating the snow water equivalent from snow depth measurements in the Swiss Alps. J. Hydrol. 378, 161–167. doi:10.1016/j.jhydrol.2009.09.021

Musselman, K.N., Molotch, N.P., Margulis, S.A., Kirchner, P.B., Bales, R.C., 2012. Influence of canopy structure and direct beam solar irradiance on snowmelt rates in a mixed conifer forest. Agric. For. Meteorol. 161, 46–56. doi:10.1016/j.agrformet.2012.03.011

Schleppi, P., Conedera, M., Sedivy, I., Thimonier, A., 2007. Correcting non-linearity and slope effects in the estimation of the leaf area index of forests from hemispherical photographs. Agric. For. Meteorol. 144, 236–242. doi:10.1016/j.agrformet.2007.02.004

Singh, P., 2001. Snow and Glacier Hydrology, Water Science and Technology Library. Springer Netherlands.

Thimonier, A., Sedivy, I., Schleppi, P., 2010. Estimating leaf area index in different types of mature forest stands in Switzerland: a comparison of methods. Eur. J. For. Res. 129, 543–562. doi:10.1007/s10342-009-0353-8

Expected date of thesis defence

2015/16 WS – FES

The Diploma Thesis Supervisor

Ing. Jiří Pavlásek, Ph.D.

Supervising department

Department of Water Resources and Environmental Modeling

Electronic approval: 10. 12. 2015

prof. Ing. Pavel Pech, CSc.

Head of department

Electronic approval: 10. 12. 2015

prof. Ing. Petr Sklenička, CSc.

Dean

Prague on 10. 12. 2015

Declaration:

Hereby I declare that I worked out the thesis on the topic “Linking snow distribution and forest canopy characteristics by way of hemispherical photography” on my own with the use of the cited literature and according the instructions of my supervisors.

In Kubova Huť on the 1st of December 2015 Jiří Roubínek

Abstract:

Snow accumulation and ablation processes are strongly influenced by forest canopy. Larger variability of snow depths and snow depletion rates are found under the canopy in comparison to open areas. However, the interactions between forest snow processes and the impacts on snowpack evolution under canopy are not fully understood.

This study investigates the temporal and spatial dynamics between the forest canopy and the underlying snow pack. A series of field areas under various canopy and elevation classes centered around Davos, Switzerland containing approximately 2000 geo-rectified (+/-50cm) and labeled points have been setup for repeatable measurements of total snow depth, new snow depth and snow depletion rates. Canopy coverage characteristics have been estimated by a variety of methods, (1) hemispherical photography, (2) manual characterization and (3) airborne light detection and ranging data. The canopy characteristics derived from these methods were analyzed for correlation to approximately 40000 manual snow measurements collected at the field sites during the 2012/2013 winter season. These methods were then intercompared and evaluated for applicability to large scale forest snow studies.

The best snow predictors among the canopy characteristics were identified and used in modeling of snow in forests. Physical based model was compared to pure statistical regression.

The thesis is linked to ongoing research of snow distribution dynamics under forest canopy within WSL Institute for Snow and Avalanche Research SLF.

Keywords:

snow hydrology, canopy metrics, light detection and ranging (LiDAR), leaf area index (LAI)

Abstrakt:

Akumulace a tání sněhu v lese je silně ovlivněno hustotou korun stromů. V lesích je mnohem větší variabilita výšky sněhu i rychlosti tání než ve volné krajině. Interakce mezi procesy v lese a ve sněhu a jejich vliv na vývoj sněhové pokrývky v lesích není plně popsán.

Tato studie se zabývá časovou i prostorovou distribucí sněhu v lese a vztahem mezi sněhovou pokrývkou a hustotou lesa. Byla vytvořena síť výzkumných ploch s různou hustotou lesa a v různých nadmořských výškách v okolí Davosu ve Švýcarsku. Síť zahrnovala celkem přibližně 2000 přesně (+/-50cm) zaměřených bodů, kde byla opakovaně měřena výška sněhu, výška nového sněhu a rychlost tání. Charakteristiky hustoty lesa byly určeny několika metodami: (1) hemisférickým snímkováním, (2) manuální klasifikací a (3) z leteckého laserového skenování. Tyto metody byly porovnány a byla analyzována souvislost získaných charakteristik porostu s asi 40000 sněhovými měřeními provedenými v průběhu zimní sezóny 2012/2013.

Mezi charakteristikami porostu byly identifikovány nejlepší prediktory sněhu a použity k formulaci modelu sněhové pokrývky v lesích. Fyzikálně založený model byl porovnán s čistým statistickým regresním modelem.

Studie je součástí širšího výzkumu dynamiky distribuce sněhu v lesích, který probíhá na Švýcarském federálním institutu pro výzkum sněhu a lavin (SLF).

Klíčová slova:

sníh, hydrologie, charakteristiky lesního porostu, hemisférická fotografie, laserové skenování (LiDAR), index listové plochy (LAI)

Content

List of abbreviations 9
1. General Introduction……10
1.1 Introduction 11
1.2 Goals 11
1.3 Hypothesis and research questions 12
2. Fundamentals……13
2.1 Snow and forests 14
2.2 Mountain forests 15
2.3 Forest and canopy metrics 16
2.4 Hemispherical photography 19
2.5 Remote sensing 19
2.6 Snow as a subject 21
2.7 Snow formation 22
2.8 Snow metamorphism 24
2.9 Snowpack 25
3. Methods and Materials……27
3.1 Research plan 28
3.2 Research area 28
3.3 Research site setup 29
3.4 Snow measurements 30
3.5 Hemispherical photography – taking pictures 31
3.6 Hemispherical photography – equipment 32
3.7 Canopy characteristics 32
3.8 Manual canopy classification 34
3.8.1 Classes description 35
3.8.2 Additional information 36
3.8.3 MCC Testing 36
3.9 Aerial laser scanning 37
3.9.1 Data 37
3.9.2 Cartesian approach processing 38
3.9.3 Synthetic hemispherical photos 38
3.10 Hemispherical photo processing 38

3.11 Hemispherical photo analysis 39
3.12 Snow data analysis 40
3.13 Snow model 41
3.13.1 Snow predictor search 41
3.13.2 Statistical model 42
3.13.2 Physical based model 42
4 Results and Discussion……..46
4.1 Snow cover characteristics 47
4.2 Hemispherical photography and canopy classification 48
4.3Manual canopy categorization 49
4.4 Snow and canopy categories 51
4.5 Canopy characteristics as snow predictors 54
4.6 Snow model 56
4.7 Cartesian LiDAR based canopy characteristics – sensitivity analysis 59
4.8 AHP derived canopy characteristics 60
4.9 Snowpack relation to HP and AHP derived canopy characteristics 61
5. Conclusions……..63
6. References……65
7. Acknowledgement……...73

List of abbreviations

AHP	Artificial/synthetic Hemispherical Photography
ALS	Arial Laser Scanning
CCL	Canopy Closure
CCL30	CCL for limited zenith view angle of 30° (similar for 60° and for LAI)
CCLS	CCL for limited azimuth angle only to south quadrant (similar for east, west, north and for LAI)
CGF	Canopy Gap Fraction
COP	Canopy Openness
CULS	Czech University of Life Sciences Prague
DL,DM	Drusatscha low resp. medium density site
DOZ	Drop-off zone
DSM	Digital Surface Model
DTM	Digital Terrain Model
ETM	Equi-temperature metamorphism
GPR	Ground Penetration Radar
HN	New snow depth
HP	Hemispherical Photography
HS	Snow depth
HSf	Snow dpth in forest
HSo	Snow depth in open
IH,IL,IM	Ischlag high resp. low resp. medium density site
LAI	Leaf Area Index
LH, LL	Laret high resp. low density site
LiDAR	Light Detection and Ranging
MCC	Manual Canopy Classification
PCA	Principal Component Analysis
PISR	Potential Incoming Solar Radiation
RHP	Real Hemispherical Photography
rHS	Relative snow depth compared to open
SLF	WSL Institute for Snow and Avalanche Research
SVF	Sky View Fraction
SWE	Snow Water Equivalence
TGM	Temperature-gradient metamorphism
TSM	Transmission

1 General Introduction

This chapter describes the main focus of the study and gives the relevance of selected topic study (1.1), formulates main goals (1.2) followed with the research questions and hypothesis (1.3).

Figure 1.1: Mountain snowy forest

1.1. Introduction

Snow accumulation and ablation processes are strongly influenced by forest canopy. Forested areas represent a significant portion of areas with seasonal snow cover. 30% of the area of Switzerland is covered by forests. These areas act as vast snow and water storage reservoirs.

There is an increasing demand for further investigation of this storage component because of hydropower production and natural hazard protection. Therefore we need to understand better the snow forest interaction to be able to assess the spatial temporal snow distribution in forests. Snowpack in forests exhibits much larger variability compared to open landscape.

This study focuses on the relation between snow distribution and canopy characteristics. It is based upon field measurements of snow cover and canopy characteristics at several sites surrounding Davos in Switzerland as well as subsequent data processing and analysis schemes. The aim of this work is to develop, test and compare methods for canopy characteristics determination using (1) hemispherical photography (HP), (2) manual characterization and (3) airborne light detection and ranging data sets. These methods are then used to compare snow and canopy characteristics (acquired from field measurements) as well as study the relationships between them.

1.2 Goals

The thesis consists of three distinct parts, which are strongly linked to each other.

The first topic is relationship between snow cover and canopy characteristics in fine scale. In order to identify and quantify this relation, the snow and canopy data were inter-compared. Snow cover characteristics were measured in very fine grid. Fine grid means a lot of points (for more detail see section 3.3 and 3.4).

Also obtaining canopy characteristics for a large set of points from real hemispherical pictures (HP) requires taking pictures at each of the points. Taking HPs is a very time consuming process, which is getting impossible for a large set of points (fine grid or large areas). That is the reason why alternative methods were studied. This was the second part - investigation of alternative methods to get canopy characteristics and a comparison of these methods with real HP.

In the last part the outcomes from previous parts were used for the snow model. The physical mass balance model for snow under the canopy was proposed and compared to simple statistical one.

The three topics mentioned above can be summarized in 3 main goals:

G1: Study the snow cover in forested sites and its relation to canopy.

G2: Study the canopy at these sites. Compare several methods.

G3: Quantify the snow-canopy relation and propose a snow model.

1.3 Hypothesis and research questions

Research hypothesis and corresponding questions were formulated according to the main goals:

H1: There is a significant correlation between snow and canopy characteristics on a small scale. This dependency can be quantified and used for a snow model.

Q1: What is the relation between snow depth and canopy characteristics? Which canopy characteristic are the best snow predictors?

H2: Correspondence of canopy characteristics obtained from hemispherical photography (HP) and from Light Detection and Ranging (LiDAR) is expected. The correlation of characteristics for various parameters will be studied.

Q2: What is the correlation of canopy characteristics obtained from HP and from LiDAR for different offsets/parameters?

H3: A mass balance approach, which considers differential snow depth data, can enhance the snow distribution model.

Q3: Is the physical (mass balance) based model incorporating differential snow depth data more efficient than direct correlation of total snow depth with canopy characteristic?

2 Fundamentals

Even if the most of the readers of this study have a good previous knowledge of snow science, it is useful to briefly remember the basic fundamentals. Present cross-subject study combines snow science, forestry and remote sensing. Experts in one of the subjects often cannot have complete knowledge of the next one. Therefore there are briefly introduced the basic fundamentals required to read this study. Furthermore the snow and canopy characteristics, used in the thesis, are defined in this chapter.

The chapter starts with general information about snow and forests showing the relevance of the study in global scope (2.1), giving basic facts about mountain forests in the Alps (2.2), canopy metrics (2.3) and methods used to acquire data for canopy metrics: hemispherical photography (2.4) and remote sensing (2.5). Further sections of this chapter are describing the snow as a substance (2.6), its formation (2.7), metamorphism (2.8) and deposition (2.9).

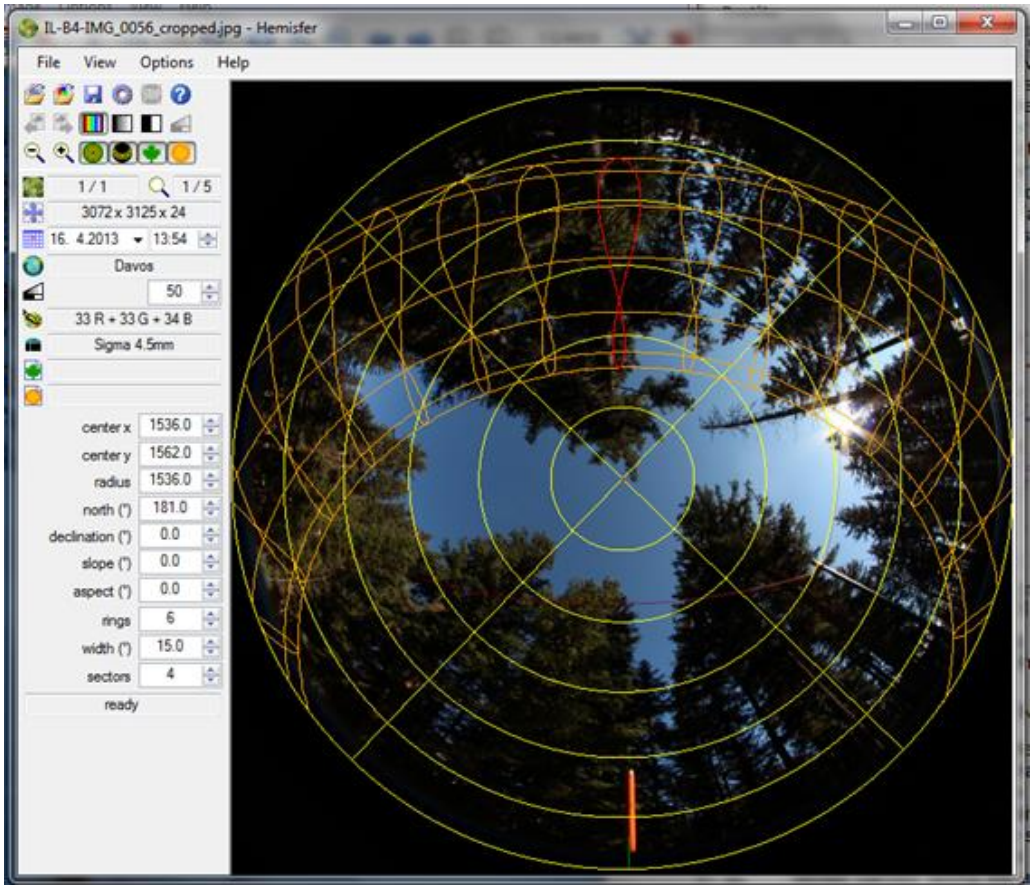

Figure 2.1: Processing hemispherical image in Hemisfer software

2.1 Snow and forests

There are several climatic and vegetation zones changing with latitude and elevation on the Earth. Forests cover a large portion of continents, especially Europe, North America and Asia. The forest zone overlaps the zone with (seasonal) snow cover as it is shown in Figure 2.2. Despite the fact that the map obviously underestimates the extent of snowy forests areas in Europe except for Scandinavia considering only boreal forests, it clearly shows that snowy forest cover a huge part of the Northern Hemisphere. Even if there are no direct estimates of the overlap between snow covered and forested areas, the boreal evergreen needleleaf forests (typical in subpolar boreal forest regions of the Northern Hemisphere) account for 8.9 million km^2, and snow may (by a conservative estimate) overlap boreal forest on 19% of the Northern Hemisphere (Rutter et al. 2009). Snowy forests stand not only for the vast boreal forests in the cold climatic zones but also subalpine and montane forests in the tempered zone. Snow in forest phenomenon plays an important role in the Alps, Pyrenees and Carpathian mountains. According to the United Nations Food and Agricultural Organization (UNFAO 2015), 31.4% or about 1,240,000 ha of Switzerland are forested, and the forested portion is (slightly) increasing by 0.3% annually. The situation is similar in Lichtenstein with 43% and Austria with 47% of forested areas.

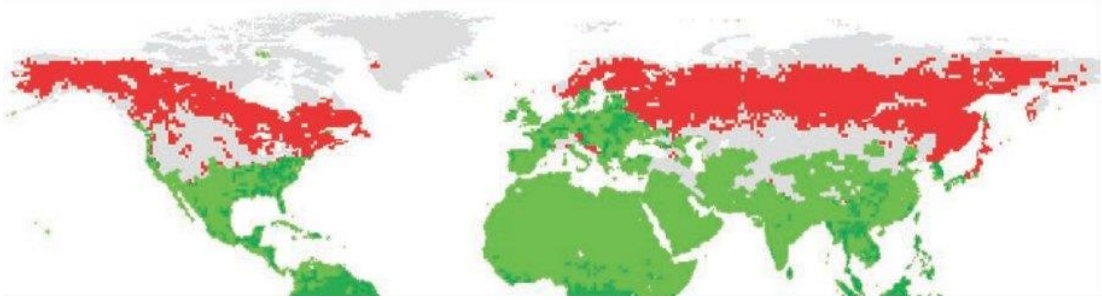

Figure 2.2: Forests with snow cover in the Northern Hemisphere in Jan 2005 (red), unforested areas with snow cover (gray), snow-free forests (dark green). (Source: Essery, R., et al. 2009)

The hydrology of forests plays an important role in the global water budget. Snowmelt dominated forested headwaters controls 60% of the global freshwater runoff (Chang 2012). The forest canopy causes much higher spatial heterogeneity of snowpack compared to open areas because it strongly influences physical processes involved in snow accumulation and ablation. The processes can be either inhibited or amplified. Thus the dynamics of snowpack in forests highly differs from open area (Jonas et Essery 2011). One of the key factors is interception, which can range from low to over 60% of total annual snowfall (Montesi et al. 2003; Storck et al. 2002).

Accurate estimation of snowmelt rate and runoff from forested areas is very important for hydrological forecasts, which are demanded by engineers in the power industry and nature hazards protection.

The snow and forest interaction is interesting also because of the global consequences. Within the Northern Hemisphere it is estimated that 20% of the seasonal snow cover is located within forested areas and can account for 17% of total

terrestrial water storage during the winter season (Güntner et al. 2007; Rutter et al. 2009). EEA (2015a) states the intensified competition for resources as one of the global megatrends we have to deal with. Also the both, water and forest (biomass) are important resources. Rosengrant et al. (2002) predicted alarmingly high global water withdrawal ranging from an increase of 18–50% in 2025. EEA (2015b) analyzes the forest water storage and flood mitigation capacity of European forests.

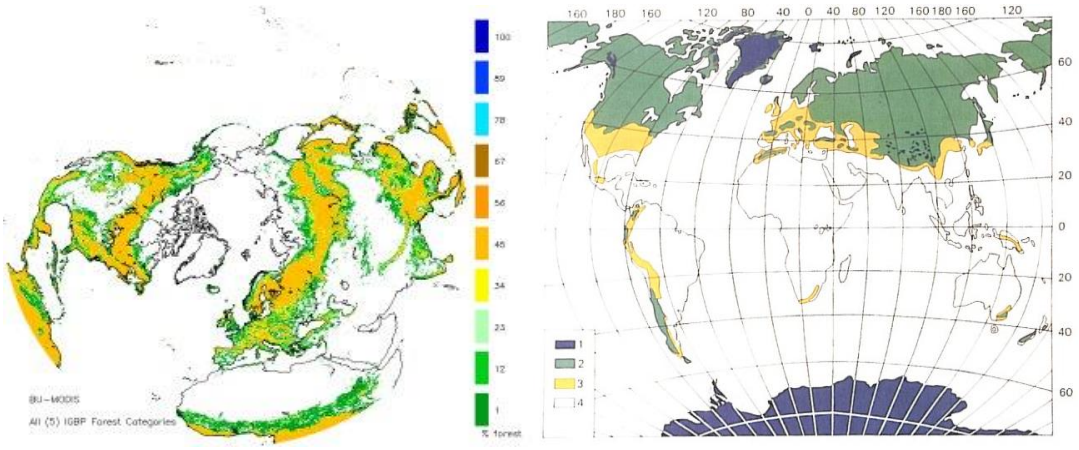

a/ b/

Figure 2.3: a/ Northern Hemisphere forest extent derived from MODIS satellite data (NSIDC 2015) and b/ global snow cower (green areas) is stable snow cover of varying duration every year and the yellow, are areas where unstable snow cover occurs almost every year (Source: Armstrong et Burn 2008)

2.2 Mountain forests

The highest locations in mountains, alpine zone, are free of any trees because of extremely harsh conditions. In the Alps, there are the temperate coniferous forests occupying the subalpine and montane vegetation zone, which are below the alpine zone. The subalpine zone is just below the tree line, the limit elevation where the trees fail to grow. Lugo, A.E. et al. (1999) defines the montane zone as having a biotemperature of between 6 and 12 °C, where biotemperature is the mean temperature considering temperatures below 0 °C to be 0 °C. Above the elevation of the montane forest, the trees thin out in the subalpine zone with the biotemperature between 3 and 6 °C. The subalpine zone is a relatively narrow belt where stunted, often infertile individuals of various tree species survive, despite blasting of windblown snow, frost damage, and desiccation.

The mountain forests (Figure 1.1) in the Alps are spruce (Norway spruce/ *picea abies*) dominated (49%). Other typical species for these forests are European larch (*larix decidua*) with 10%, and pine (*pinus sylvestris*) and Swiss stone pine (*pinus cembra*) with also 10% portion together. In lower altitudes, fir (*abies alba*, 4%), beech (*fagus sylvatica*, 8%) and maple (*acer*, 4%) can be mixed in (Brändli et al. 2015) Afforestation percentage value varies from 25% to 52% in Switzerland. Figure 2.4 shows that higher values are related to the southern part of the Alps. Also the increase of forested area is higher in the south (WSL 2007).

The forests play an important role in hydrological processes as a water storage controlling run off from headwater catchments. Also changes of micro climate and of energy fluxes caused by the forest canopy are of great importance. EEA 2015b)

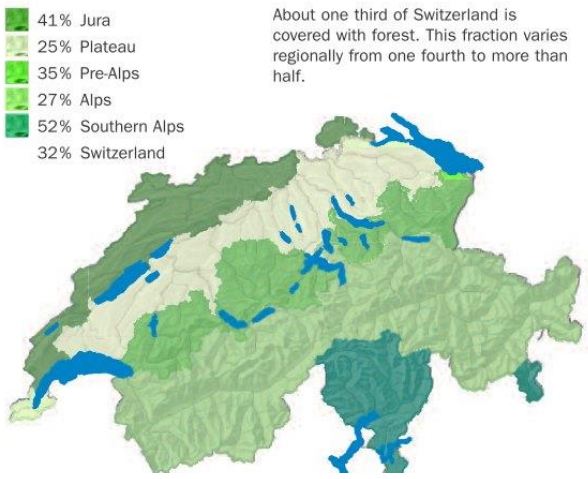

Figure 2.4: Afforestation of Switzerland in 2015 (WSL 2015)

Around 80 percent of drinking water in Switzerland is obtained from groundwater. The seepage water from forest soils is particularly important for its supply (FOEN 2015).

Waring (2002) states that evergreen coniferous forests reduce stream flow by an average of 15 – 25% in comparison to deciduous hardwoods in similar environments thanks to high annual water vapor transfer from their well ventilated dense canopies. The dense, finely dissected canopies of evergreen conifers also have the propensity to condense water (and pollutants) from clouds, leading to fog drip, which can increase the effective precipitation at high elevations substantially in windy environments (Ham 1982). Water stored in the sapwood of conifer trees can serve as a temporary buffer against drought. During the day, this reservoir may contribute up to a third of the water transpired, with refilling during the night. The ratio of sapwood mass to leaf area increases in conifers with harshness of the environment (Waring and Running 1978); the total volume of sapwood determines the reservoir of water.

All the forest related phenomenona and processes, like interception; evapotranspiration; sapwood water storage; melt rate reduction; moisture condensation etc., result in stream runoff stabilization and (high and low) peak runoff reduction.

2.3 Forest and canopy metrics

Forests are not a homogenous environment; exhibiting a very heterogeneous spatial structure. Several standard metrics were developed to quantify several forest variable properties. The following overview cannot be the complete list. For more details see e.g. (Cornelius et al. 2004; Brack 1999; Brack 2000; Jennings 1999).

Large groups of metrics were developed for use in forest inventories. Many of them are focused on the assessment of forest growth and yield, description of parameters important for wood production and estimation of the value and possible uses of timber: DBH-diameter at breast height (1.3m), tree height, age, the number of trees per ha (stem density), the basal area, site index (a species specific measure of site productivity and management options, reported as the height of dominant and co-

dominant trees in a stand at a base age such as 25 years), the volume of trees in an area, and annual volume (or diameter) increment.

Unlike the forest inventories interested in the timber production capacity this study is interested in canopy characteristics describing the forest canopy structure and density. Such kind of measurements came up with increasing concern over ecology, biodiversity and sustainable development during the last decades. For instance the leaf area index (LAI, definition see below) measurements were often motivated by an effort to quantify the photosynthetic process, which is related to the active surface of leafs. Active surface plays an important role also in evapotranspiration. LAI directly quantifies canopy structure, and can be used to predict primary productivity and crop growth. It is commonly used in ecosystem models because it has an important influence on exchanges of energy, water vapor and carbon dioxide. LAI correlates well to vegetation indexes (NDVI, EVI) gained from satellite imagery (Carlson et Ripley 1997).

The advance in technology allowed fast development of measuring and analytical methods resulting in the current high research interest in the application of remote sensing techniques in this field.

Canopy structural parameters are often used to give an adequate representation of vegetated ecosystems for various purposes including primary productivity, climate system, water and carbon gas exchanges, and radiation extinction. Canopy structural parameters are usually described using several pseudo-synonymous terms, often measuring different components of vegetation canopies. Standardization in the definitions has fallen short, leading to a confusion of terms even in standard text books making the comparison of historic measures futile (Gonsamo et al. 2013).

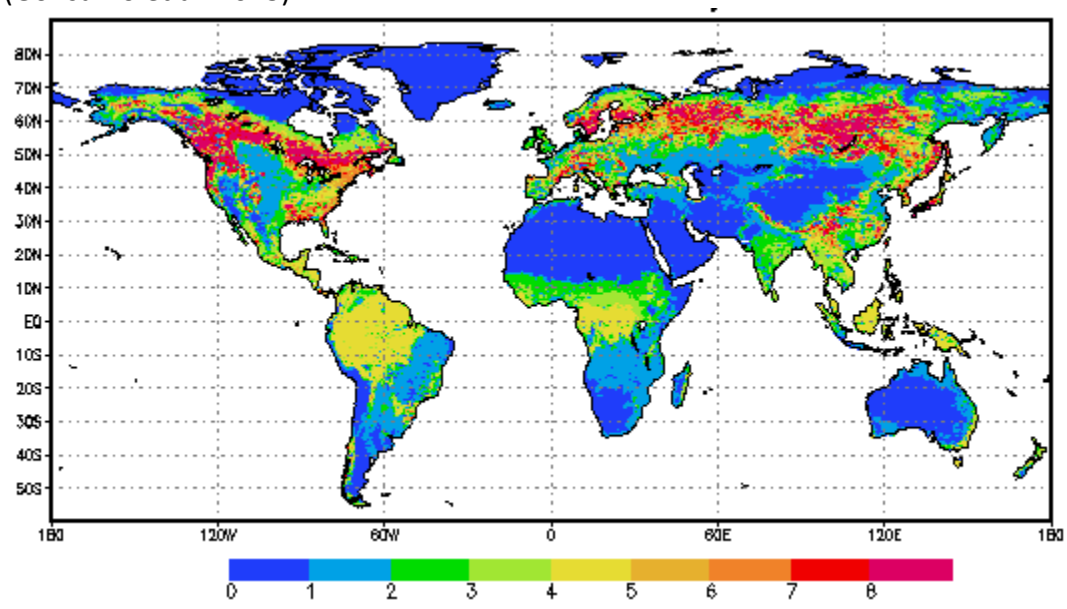

Figure 2.5: LAI distribution in the world (NASA 2015)

Let's make a short overview of commonly used canopy characteristics and their definitions: leaf area index (LAI); foliage density; canopy closure (CCL), gap fraction, sky view fraction or factor (SVF), transmission, fractional cover, and canopy openness. The long list is a bit confusing. But it can be easily reduced to get a

much smaller set of parameters because the list contains many equal or complementary properties as the following description shows:

The leaf area index (LAI) of a canopy is quantity describing foliage density. It is defined as (upper) leaf area per unit of ground area. In other words, it tells us how many layers of leaves would be on the ground if they would all fall down and be arranged exactly side by side on the ground area below the tree crown. Or very simply it tells the average number of leaf layers above the point under the tree. Figure 2.5 gives an overview of LAI world distribution estimated from satellite imagery. Even if the LAI is greater than 1 (Figure 2.6), there is still some free space among them allowing the light to reach the ground. That is because the leaves are not organized side by side into impermeable sheet but they are arranged more or less randomly (Schleppi et al. 2007, Weiss et al. 2003).

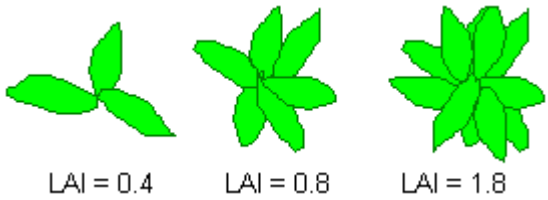

Figure 2.6: LAI description (kurtz-fernhout.com 2015)

Light transmission, often called only transmission, refers to the light reaching the ground under the canopy. Transmission is expressed as a percentage value. Complementary property would be light interception. The light conditions in the forest understory are fundamental for many processes related to vegetation cover (Da Silva et al. 2011). We assumed that the light quantity drives also snow processes like settling and depletion. Estimating light quantity in the forest understory is not so easy (Lieffers et al. 1999; Stenberg et al. 1999). The visual assessment and also sensor measurements are strongly biased by the meteorological conditions, the daytime, and the solar pathway (Pukkala et al. 1993). Since the pioneering work of Monsi et Saeki (1953), many models simulating light interception and transmission by plant canopies have been developed – for review see (Myneni et al. 1989)

Canopy closure (CCL) is another metric that is commonly used in characterizing canopy structure and is defined as the proportion of the sky hemisphere obscured by vegetation when viewed from a single point (Jennings et al. 1999)

However fractional cover (FCO) is sometimes defined equally as CCL (Gonsamo et al. 2013) or equally to crown cover (Morsdorf et al. 2006). More frequently (vegetation) fractional cover refers to land cover and means the proportion of an area that is covered by each member of a predefined set of vegetation or land cover types.

Canopy openness (COP) is complementary to CCL and characterizes the light availability under the canopy. Sprugel et al. (1996) defines COP as the unweighted fraction of unobscured sky. According to Stenberg et al. (1999) COP does not correlate with LAI.

Canopy gap fraction (CGF) is the fraction of view in some direction from beneath a canopy that is not blocked by foliage, which is the same as COP. And that is equivalent to sky view fraction or sky view factor (SVF) defined as the ratio of the visible portion of sky to total sky hemisphere (Gladt et Bednar 2013).

Crown closure, also known as crown cover, is the percentage of ground covered by a vertical projection of the outermost perimeter of the crowns in a stand. Brack (2001) and Korhonen et al. (2011) call this parameter vertical canopy cover to distinguish it better from angular canopy closure (CCL).

2.4 Hemispherical photography

The forest canopy is complex tree dimensional structure and the direct quantification of its properties is very tedious and time consuming process typically involving destructive sampling. Therefore indirect methods like hemispherical photography, the LAI-2000 plant canopy analyzer, a ceptometer or a spherical densitometer, have been developed. They are commonly used and considered as the standard methods to obtain canopy characteristics.

The basic principle of HP is taking pictures by the use of an upward looking camera with a fish-eye lens capturing the entire hemisphere above the camera. Acquired pictures are analyzed in subsequent process of image classification (to distinguish sky and foliage in case of forestry applications) and a calculation of the searched characteristics.

Hill (1924) constructed whole-sky lens (also known as a fisheye or hemispherical lens nowadays) for use it in meteorological sky observation and cloud formation study. The first hemispherical photography (HP) application in forestry published Evans et Coombe (1959), who used it to estimate sunlight penetration through forest canopy openings. Even if HP analysis required a lot of tedious manual work by scoring of overlays of sky quadrants and the track of the sun, film HP has been used for a long time to estimate forest canopy properties and light regime under the canopy (Anderson 1964; Anderson 1971; Bonhomme et al. 1974).

However wider adoption of HP came with the advent of computer technologies and digital photography, which greatly simplified the process of image acquisition and analysis. Jonckheere et al. (2005), Leblanc et al. (2005) and Ryu et al. (2010) confirmed high accuracy of HP in gaining the canopy characteristics. Moreover many software tools were developed Gap light analyser - GLA (Frazer et al. 1999), Hemiview (Webb 1999), Hemisfer (Schleppi et al. 2007) (Figure 2.1), CAN_EYE, WinSCANOPY, RGBFisheye, CIMES-FISHEYE etc. On the contrary, Jonckheere et al. (2004) mention the remaining difficulties in HP: accurate and meaningful estimates of forest canopy properties with digital hemispherical photography are hindered by different critical steps, regarding image acquisition and software processing; thus, adequate field collection and image processing procedure is required to achieve the standard of an ideal device. Chianucci et Cutini (2012) provided wider review of HP dealing also with current drawbacks of the digital HP method.

2.5 Remote sensing

Webb (1999) describes HP as an upward looking remote sensing. Remote sensing is generally defined as an acquisition of information about an object or phenomenon by observing or measuring them from a distance. The blurred term

‘from a distance’ keeps some freedom in setting up the border between in-situ measurement and remote sensing but remote sensing typically refers to the scanning of the earth by sensors mounted on satellite, aircraft or other flying device like drones or balloons.

The sensors gain information about objects reflectance or emissivity in predefined frequency range (spectrum) of electromagnetic radiation. Remote sensors can be either passive or active. The passive sensor records natural energy, the most common reflected solar radiation. In contrast, active sensors use internal stimuli to collect data about the surface.

LiDAR stands for light detection and ranging (NOAA-NGS 2015) or for laser imaging, detection and ranging (Bauhahn,et al. 2009). Compare to radar standing for radio detection and ranging. LiDAR refers to active sensor measuring the distance by illuminating a target with a laser beam and analyzing the reflected signal. This technique is also alternatively called laser scanning or laser altimetry. It can be either airborne (or spaceborne) or terrestrial.

Revuelto et al. (2014) and Kukko et al. (2015) used terrestrial LiDAR for snow survey. Terrestrial LiDAR produce precise continuous information about snow height in selected area. This method provide good results in open landscape but the usage of terrestrial LiDAR in forests is limited because of tree shading.

Aerial laser scanning (ALS), which is equal to airborne LiDAR, is a perfect method to gain the digital terrain or surface model (DTM or DSM). DTM is a topographic model of the bare earth and DSM represents surface of terrain with all objects (buildings, vegetation etc.). Availability and accuracy and usage of digital elevation models (DEM is the generic term for DTM and DSM) are currently rapidly increasing in Europe. Schaer (2010) delivered the current ALS technology review and discussed the challenges related to the calibration of the ALS system.

Deems et al. (2013) and Helfricht et al. (2012) used airborne LiDAR to study the snow height distribution. Korhonen, et al. (2011), Morsdorf, et al. (2006) and Solberg, et al. (2009) estimated forest canopy LAI from airborne LiDAR and Wang et al. (2004) and Haboudane (2004) used MODIS satellite data for LAI estimation.

Remote sensing means not only the data acquisition but also the data processing (removing the influences of atmosphere etc.) and post processing (image classification and interpretation). For remote sensing synthesis see (Tupin et al. 2014; Richards 2013; Schowengerd 2012). Dietz et al. (2012) and Hall et Martinec (2012) summarized the available methods in remote sensing of snow. Seidel et Martinec (2004) focused on the remote sensing in snow hydrology and runoff estimation.

2.6 Snow as a subject

I am repeatedly asked by many people: ‘why study snow?’ They always tell me that ‘it is just frozen water, nothing extraordinary.’ On the other hand, every child tells that ‘no two snowflakes are alike.’ Children and scientists see snow as a magic substance exhibiting large variability of its properties. Snow is able to be either soft or hard, either brittle or elastic, either solid or flowing, either fluffy or dense, either porous or impermeable, either dry or carrying high liquid water content. Also the arctic native people, like Inuit or Sami, experience the snow diversity in everyday life and their languages reflect it by a high number of expressions for snow.

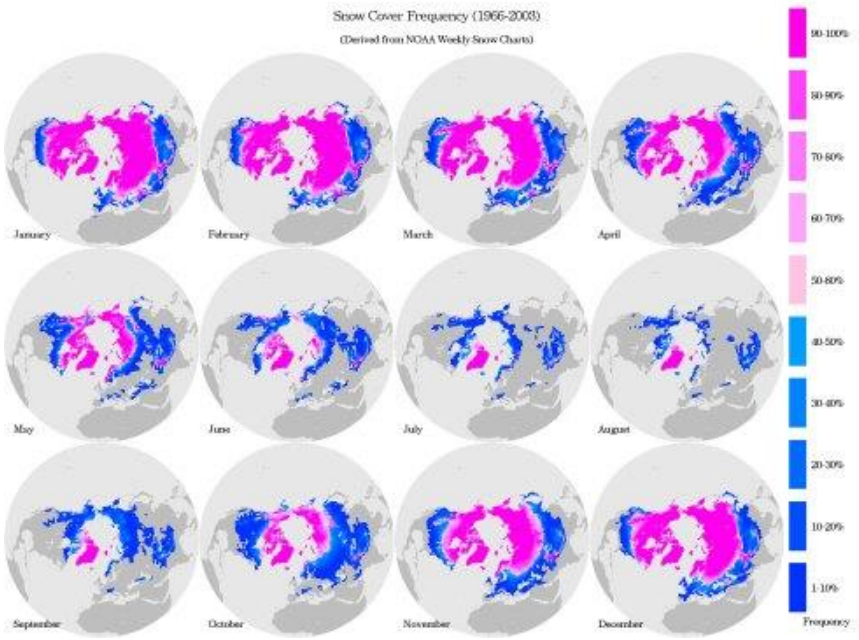

Figure 2.7: Snow cover frequency (1966-2003) based on NOAA satellite data shows average snow cover fluctuations during the year (NSIDC 2015)

Snow is a mixture of frozen water crystals and air locked among them. Snow forms as precipitation by vapor freezing in atmosphere. After falling down it accumulates on a surface in a layer structured snowpack. Snowpack development is influenced by several factors: snow transformations, erosion and redistribution by wind drift, settling, energy and mass exchange on surface.

Snow is of high importance in the water cycle, runoff formation and stream discharge regime. Even if the snow cover area and duration in the Northern Hemisphere is decreasing due to climate change (Brown et Mote 2009), about 42% of land in the Northern Hemisphere is exposed to seasonal snow cover with a significant duration (Dingman 2002) (Figure 2.3). Figure 2.7 shows variability of snow cover in Northern Hemisphere during the year.

2.7 Snow formation

Snow formation in the atmosphere requires an air oversaturated with water vapor and low temperature. Saturation pressure decreases nearly exponentially with the temperature, which is decreasing (more or less linear in troposphere) with elevation. In other words, the warmer air in lower layers of the atmosphere can hold much more vapor than the higher ones. The oceans play the role of the largest moisture source in global water cycle. Atmospheric circulation brings the moist air to the continents (Figure 2.8). When the warm moist air is lifted up, it adiabatically cools down, becomes oversaturated and clouds start forming. Upward air movement can be caused by cyclonic convergence (upward air flow around the center of low pressure area), frontal lifting (at atmospheric front), orographic lifting (in mountains) or convection (thermally induced vertical motion). The dust particles, taken by wind from earth surface and transported to the atmosphere, work as condensation and ice nuclei. Unlike condensation, the nucleation process is restricted to small portion of aerosol particles which are similar to ice and has a larger size (0.1 - 15 μm) (Armstrong et Brun 2008).

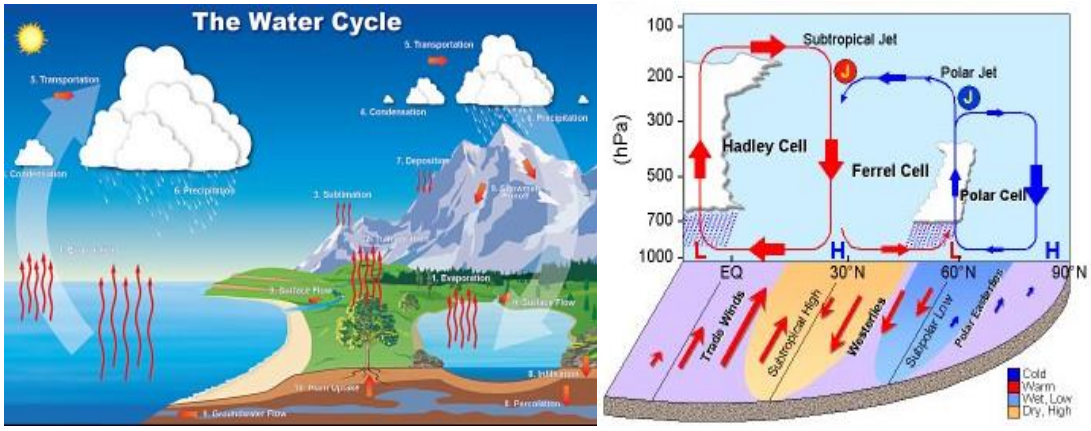

a) b)

Figure 2.8: Global a) water cycle (NOAA 2015) and b) atmospheric circulation (WeatherBELL Analytics 2015)

When the cloud temperature drop to about -5°C, the active nuclei present in the atmosphere create tiny (about 75 μm) ice crystals. This process is called ice (heterogeneous) nucleation. Homogenous nucleation, involving no other substance like water (vapor), is very rare because it requires temperatures below -40°C, when minute ice particles can be formed by a chance combination of molecules. Ice crystals are the initial stage in snow crystal growth which involves several processes as follows: accretion (vapor deposition on crystal planes), aggregation (adhesion of snow crystals after their collision), riming (the water droplets coming in contact with the falling crystal) and multiplication (mechanically weak crystals brake into pieces, which continue growing separately). The grow rates on basal and prism planes depends on temperature and supersaturation (Figure 2.9). The crystal growth in mixed (water and ice) clouds can be intensified by the coagulation process when

crystals grow quickly at the expense of water droplets due to higher vapor pressure above water than ice surface.

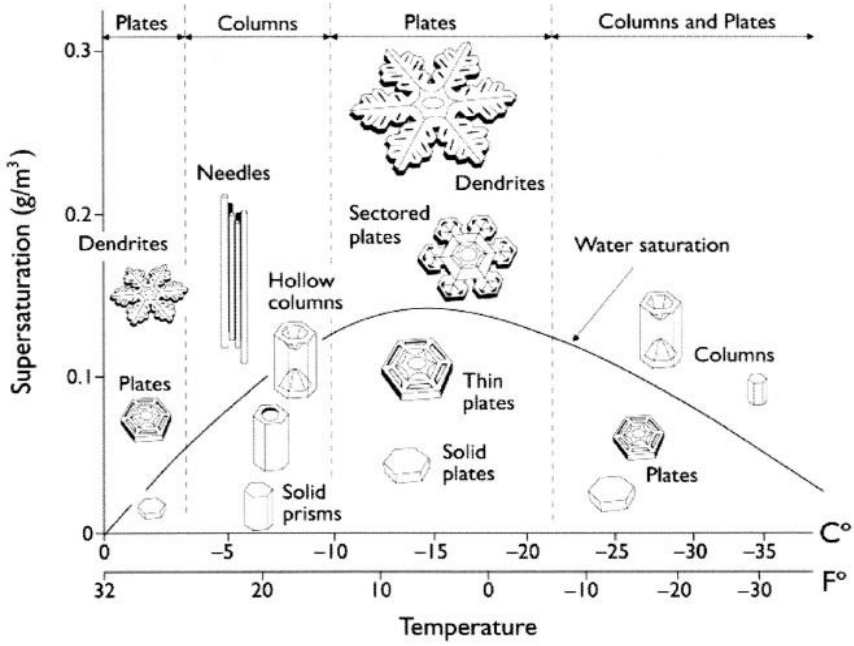

Figure 2.9: Snow formation diagram: Temperature and supersaturation determine grow rates on basal and prism planes influencing the shape. The size is influenced by intensity of the coagulation process depending on the difference in vapor pressure between water and ice surface. The difference is shown by the supersaturation curve. (Armstrong et Brun 2008)

In a typical cloud a 1mm snowflake can grow to 10mm in 20 minutes (and can transform into a 1mm droplet when it is melted). The snowflakes are irregular aggregates of about 10-100 crystals (usually dendrites and plates) and their size can reach up to a cm in length. While the individual crystals size is 50μm – 5mm at the earth surface (Hobbs 2010). Variability of conditions and process combinations results in variability of snow crystal forms.

Figure 2.10 describes where the hexagonal structure of snow crystals comes from. Water (H_2O) molecules create a hexagonal lattice - each water molecule has four neighbors (in 3D) so it acts as a hydrogen donor to two of them and a hydrogen acceptor from the other two. Growing single crystal keeps the shape, because it is easier for molecules to stick to a rough surface than a smooth one because a rough surface offers more sites where a new molecule can bond to several of the surface molecules at once. The structure grows into a hexagonal prism, which is the basic ice crystal form – a brick for building any snow flake (prismatic or dendritic).

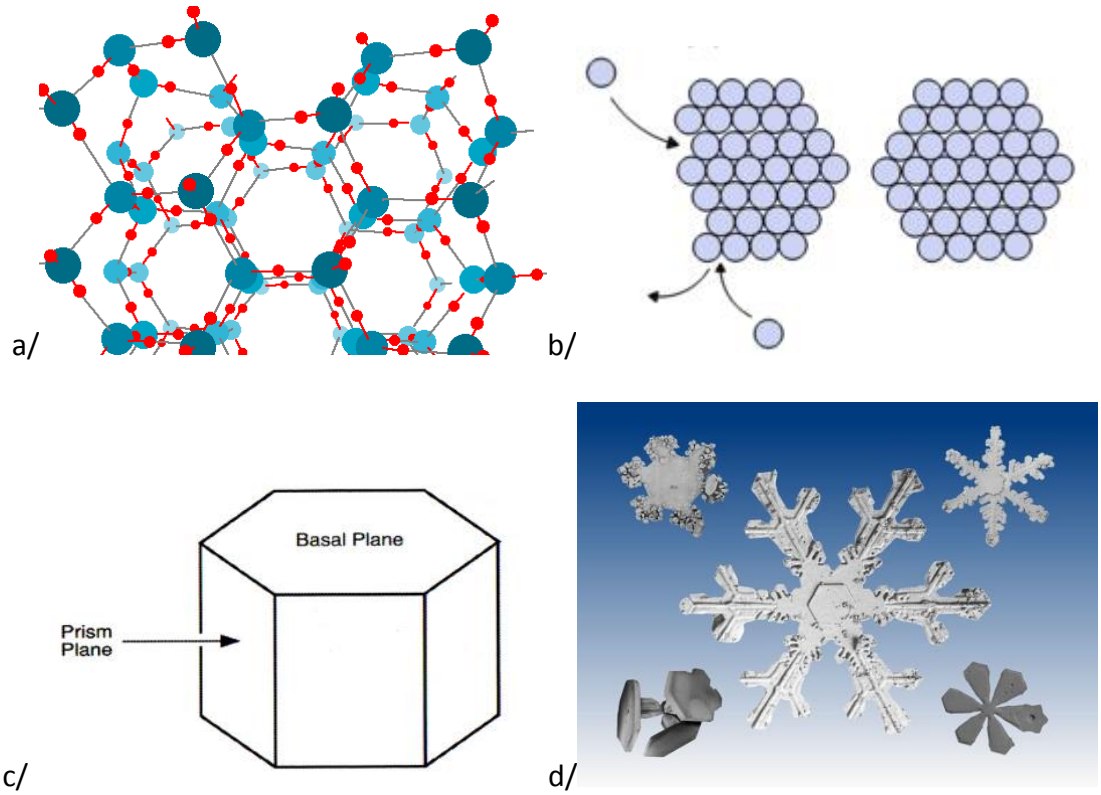

Figure 2.10: Hexagonal structure: a/ of ice molecular lattice (Kalma 2015) and b/ growing ice crystal keeping the shape and building (Smith 2015) c/ the hexagonal prism (Armstrong et Burn 2008) – a brick for building any d/ snow flake (Libbrecht 2015).

2.8 Snow metamorphism

Snow has been changing its form according the ambient conditions to since it was born by ice nucleation all the way down from clouds. It keeps transforming after deposition on the ground. Wind and gravitational settling cause breaking the weak crystals mechanically. Large active surface of snow crystals leads to intensive mass and energy (heat) fluxes on ice-air interface. Character of fluxes an d snow metamorphism is determined by temperature conditions.

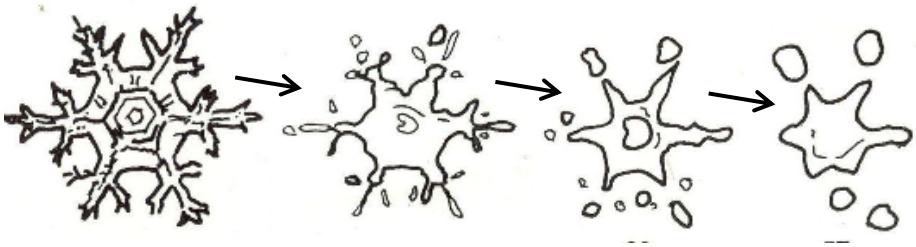

Figure 2.11: Crystal rounding by equilibrium metamorphism (Based on naturfare.no)

Equi-temperature metamorphism (ETM) is also called equilibrium or destructive metamorphism. ETM is typical for low temperature gradient (< 5 K/m) in snowpack. Vapor diffuses along its pressure gradient from convex surface, above which the vapor pressure is higher, to concave spots. This causes rounding of crystals (Figure

2.11). Complex shapes are transformed into spherical particles, concave to convex. The free energy decreases due to the reduction of surface area.

Temperature gradient metamorphism (TGM), or kinetic or constructive metamorphism, is triggered and driven by high (> 5 K/m) temperature gradient in snowpack, which often occurs in shallow snowpack during bright nights due to intensive radiative cooling of snowpack surface. Mass (vapor) flux goes from the warmer area with higher saturation vapor pressure to the cooler part above, where new crystals – facets grows (Figure 2.12).

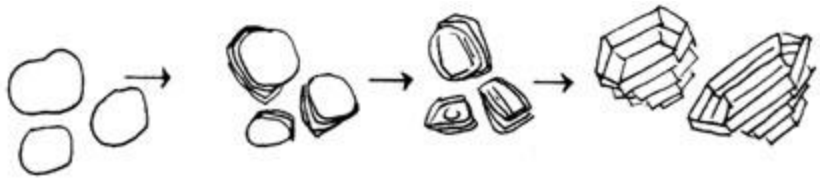

Figure 2.12: Faceting by temperature gradient metamorphism (Canadian Avalanche Association 2015)

Melt-freeze (MFM), or wet snow, metamorphism occurs mainly in the spring, when the snowpack temperature reaches the melting point due to solar radiation, warm air or rain. Snow starts thawing. Liquid water accumulates in concave spaces because of lower surface tension and creates rounded forms when refreezes during the night.

Metamorphic processes varied with temperature conditions, which changes over time and space. This variability and chaining of processes could create very complex structure. For more about these processes and their consequences for snowpack stability see e.g. (Munter 2014; McClung 2006).

2.9 Snowpack

Snowflakes fall down as snow precipitation, which are distributed by wind, intercepted by vegetation and finally deposited on the ground. Deposited snow goes through transformations and settled during the time, sublimate or melt and could be eroded and redistributed by wind. Snowpack comprise the net accumulation of deposited snow resulting from snowfall, ice pellets, hoar frost, glazed ice, refrozen rain water and contaminants.

International guidelines for classification of snow on the ground is in (Fierz et al. 2009), which is a revised version of (Colbeck et al. 1990). There are many snow characteristics, like snow height, density, humidity, temperature hardness, grain size, grain type, shear strength etc., which can be used to arrive to complete description of snow. Moreover snowpack exhibits complex vertical structure. It consists from layers piled one on the other. And each layer has different characteristics. For more details about profile measurement and modeling see (Fierz et al. 2009; Singh,et Singh 2001 and Lehning 2002).

Hydrologists usually consider the snowpack as water storage in the water cycle. Therefore it neglects the inner snowpack structure and focuses on quantification of

total snow amount using snow height (HS) and snow water equivalent (SWE). Alternatively also height of new snow (HN) is added (like in this study) to estimate the last increment, the last storm. SWE refers to liquid equivalent precipitation amount (in mm). SWE is product of HS and (mean) density. SWE is more suitable to estimate the water storage volume but on the other hand it is more difficult to measure SWE than HS.

3 Methods and Materials

This chapter starts, same as the project work, with research plan proposal (3.1). After the site setup (3.3) in the research area (3.2), snow measurements (3.4) were conducted during the entire winter season. Subsequent sections describe classification of canopy properties (3.7) and various methods used to gain them: manual canopy classification (3.8), aerial laser scanning (3.9) and hemispherical photography (3.10 and 3.11). The last sections are about subsequent data analysis (3.12) and modeling (3.13).

Figure 3.1: Field work in snowy forests

3.1 Research plan

The work on this study was done according to the research plan which was set up at the very beginning of the project:

It was necessary to finalize the setup of sampling sites before the measurements started in December 2012. (More about sampling sites see in the next section.)

Data acquisition phase was primarily comprised of snow observations in the field. Field measurement campaigns during the entire snow season were significant part of this work. Snow depth and snow water equivalent data were collected by manual measurements and GPR (ground penetration radar) measurements.

Canopy data acquisition had two parts – taking hemispherical pictures of the canopy and manual classification of the canopy. The hemispherical photography required some preparation in regards to the development of the tripod conversion setup for the hemispherical camera as well as selection of suitable methodology for taking pictures. Furthermore, an appropriate methodology for manual classification was specified (including a class set definition). (Data acquisition methods are described in sections 3.4, 3.5, and 3.8)

Data processing and analysis followed after the field measurements. It involved hemispherical picture processing, canopy data analysis and snow data analysis. Hemisfer software (provided by WSL) was used for hemispherical picture processing and obtaining canopy characteristics. The characteristics from the hemispherical photographs were compared to both the manual classification and the LiDAR data. The canopy and snow data was used in development of a point model of snow cover under forest canopy. (See sections 3.7 – 3.13 for details about data processing and analyses.)

3.2 Research area

The data analyzed in this study comes from measurements at 9 sites surrounding Davos (46.8045° N, 9.8367° E) in eastern Switzerland (Figure 3.2). Two reference open sites and seven forested sites cover a large distribution of canopy density and several altitude bands. Sites with minimal slope were chosen to reduce influence of other topographical factors (slope and aspect) in order to focus solely on vegetation and altitude influence. The sites were sorted into 3 generalized groups according to average canopy density and elevation (Table 3.1).

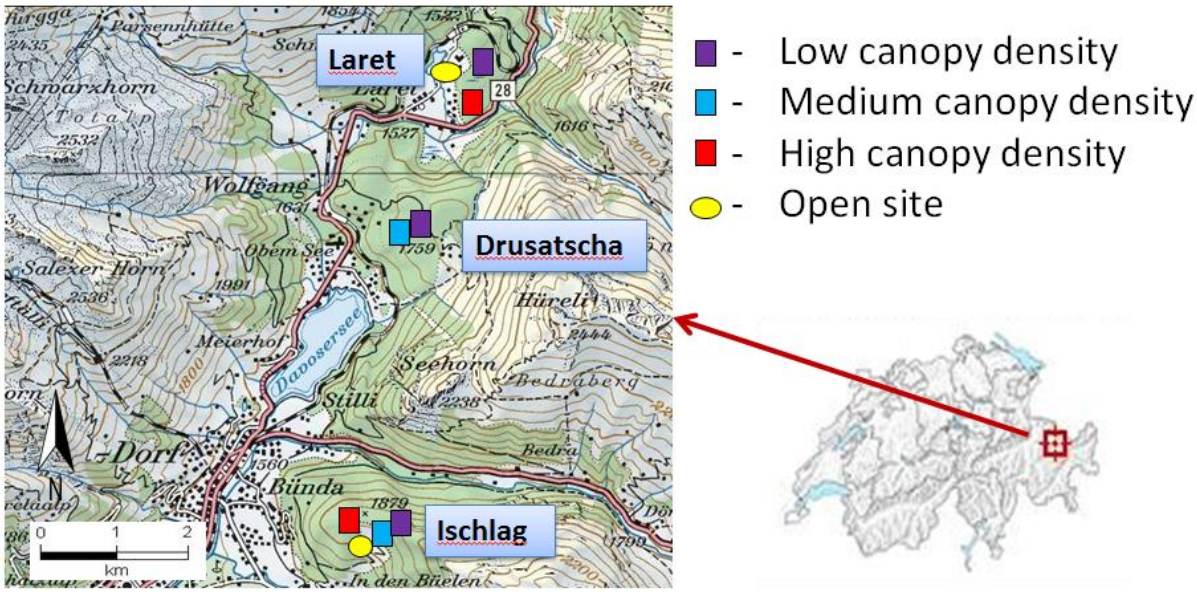

Figure 3.2: Map of measurement sites

Site	Elevation (m.a.s.l.)	Canopy density			
		Low	Medium	High	Open
Laret	1540	V	X	V	V
Drusatcha	1760	V	V	X	X
Ischlag	1870	V	V	V	V

Table 3.1: Site overview

3.3 Research sites setup

Forested research sites were 50 x 50 m square areas in subalpine coniferous forest. Precisely geo-located measuring net was set up at each site. 6 lines from north to south and 6 lines from west to east divide the area into 25 quadrants, which are 10 x 10 m each of them. Lines are attached to poles placed at each crossing point (every 10 meters). There were sampling points every 2 meters along the lines and are marked on the string for a total of 276 per site. All poles in the measuring grid were located by a DGPS (Differential Global Positioning System) giving a total error for all points per site of +/-50cm. The poles are labeled from A0 (south- east corner) to F5 (north-west). Points name like a0-14, b4-00 are used to reference all 276 points per site. System of pole labels and point names is clearly illustrated in Figure 3.3. Abbreviations of site names are used when it is necessary to distinguish the same point at different sites: Drusatscha Low – DL, Drusatscha Medium – DM, Ischlag High - IH, Ischlag Medium - IM, Ischlag Low - IL, Laret High - LH, Laret Low - LL.

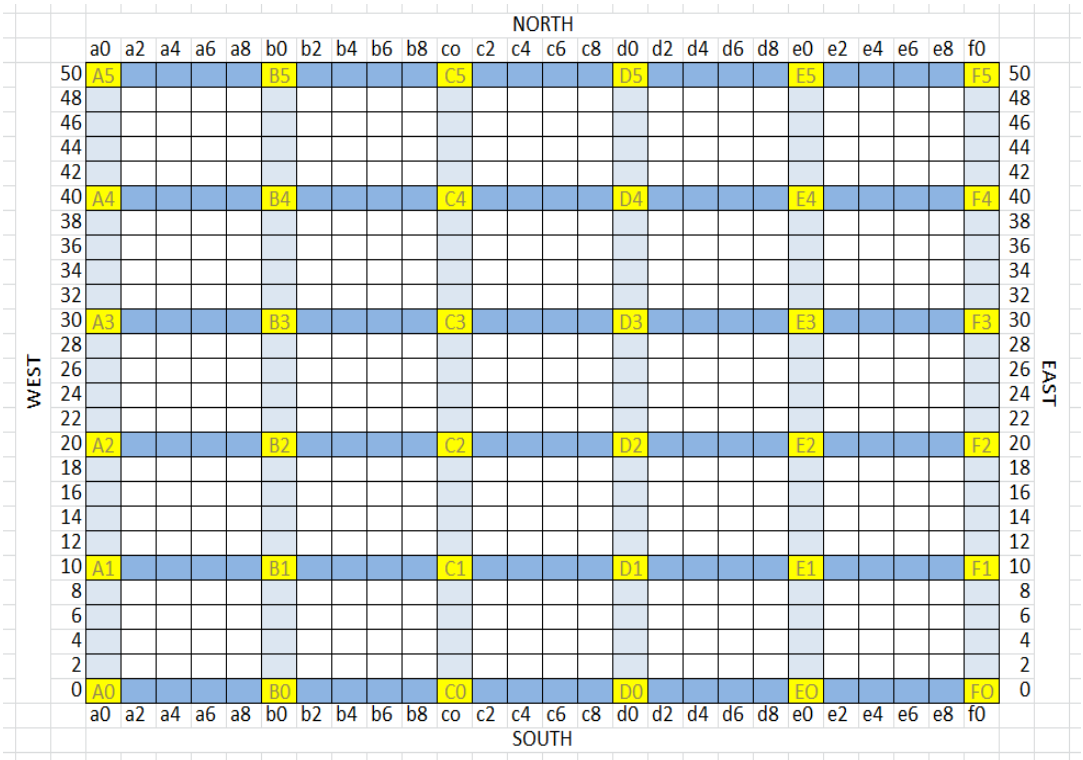

Figure 3.3 System of pole labels and point names used to identify the points within each site

There were two referential sampling transects at open sites, one located near the low elevation forested sites and the other adjacent to the high elevation forested sites. The 50 m long straight transect with 26 sampling points were stake out by three poles. Sampling points were localized using the snow probe to measure 2 m distance between points.

3.4 Snow measurements

Snow depth (HS) and snow water equivalence (SWE) values were taken in measuring campaigns during the whole snow season 2012/2013 (Figure 3.1). Two different timing schemas were applied during the season. During the accumulation period, the timing of campaigns was storm driven (measurement was conducted always after snow storm event). And for the ablation period, timing schema was switched to regular with a week period.

HS was measured manually using the snow probe at all 276 sampling points per each site. When the conditions were favorable to recognize the interface between new and old snow by probing the HS, two values – new (total storm) snow depth (HN) and total HS – per point were taken. Otherwise only total HS was measured. The interface recognition requires the jump in harness between old and new snow, ideally kind of crust. Never the less there was always some probability, that the crust had not developed at some points and some of older under laying crust was measured at those points. This could cause a bias of HN measurement.

SWE was measured manually using a US federal snow sampler at 12 fixed sampling points per site: A0, A3, A5, C5, F5, F2, F0, D0, E4, D3, C2 and B1. SWE

sampling point was moving along the spiral around the related measuring point from campaign to campaign to avoid using the spots influenced by previous measurements. The US federal snow sampler is constructed as a long metal tube with cutting ring on one end. It was screwed in to the snowpack and approximately 1 cm of underlying soil. The soil was removed from the sampler before weighting it. SWE is the weight divided by constant representing the water density and the inner area of tube.

Unfortunately the US federal snow sampler had not been available at the begging of the season. Therefore the SLF sampler had been used before US sampler was delivered. Measuring by the SLF sampler is more time consuming and disturbing larger area, because it requires digging a snow pit. Therefore SWE measurement had been restricted to only at 4 representative spots during this initial phase. Due to the destructive effect of this sampling, the measuring spots had been changed for each campaign and they always had been out of standard spots, which were used afterwards for sampling with tube sampler.

In addition HS and SWE were measured by Ground Penetration Radar (GPR) during several campaigns. GPR measurements were conducted for all transects on perimeter of the measuring grid using GPR platform adapted for using in forested sites at SLF. The GPR measurement gives the continuous information about HS and SWE. The GPR data were used primarily for other studies.

3.5 Hemispherical photography – taking pictures

It was decided to take pictures at all inner points of the measuring net at each site (for a total of 16 per site) because taking hemispherical pictures is too time demanding process and it was not possible to take pictures for all 276 points per a site.

Pictures were taken approximately 1.2m above the ground in May 2013 under low light conditions to favor the sky-canopy contrast (Fleck et al. 2004). Camera auto focus was switched off and the lens was manually focused to the infinity. ISO value was set to 400 to minimize the noise in photos. Exposure time and aperture value was set manually. The aperture value 8 was used. The probability of a reflections occurrence increase with the higher aperture values. On the other hand the low aperture values limit the ability to get underexposed photo, which is wanted because of better sky-canopy contrast. Exposure time to get the underexposed photos was determined using the following method: set the measuring mode to spot measuring, measure the exposure time value pointing the camera to the open sky, reduce the measured value dividing by 2 and set up obtained value in camera manual exposure mode. This exposure set up was used without changing for the whole site. 2 second self-timer was used to avoid shaking the camera by capturing the photo. For an example of the hemispherical picture see Figure 4.4.

3.6 Hemispherical photography – equipment

A DSLR camera Canon 600D with fisheye lens Sigma 4.5mm F2.8 EX DC HSM Circular Fisheye mounted on tripod Manfrotto 190XB with 804RC2 head and the special conversion unit. The conversion unit was designed within this project and allows mounting camera in upward looking position, quick leveling and orientation to north. Additional requirements were identified to get user-friendly instrument (which is easy to use in the field):

- Minimize the weight and size due to easy transport,
- Keep the flip-out camera display accessible,
- Easy (un)mounting the camera,
- Integrated water level and compass for easy positioning,
- Colored north arrow for easy identification in pictures,
- Keep it simple and robust enough for easy using in the field.

Figure 3.4 shows the final product. Other alternative solutions (units available to buy or to rent) were either heavier or missing some part (like north arrow or compass). This base unit met all requirements stated above. (Thanks to SLF workshop for fast and perfect construction.).

a/ b/

Figure 3.4: The HP conversion unit a/ disassembled and b/ used to mount the camera to tripod

3.7 Canopy characteristics

The basic overview of canopy characteristics is in the section 2.3 Forest and canopy metrics. Three of them, CCL, transmission and LAI, were selected as the representative canopy characteristics and potential snow predictors in this study. It seemed to be pretty simple, but closer view shows that there were few hidden questions waiting for an answer: How the calculation deals with canopy structure irregularities like leaf angle and canopy clumping? Which calculation method should be used if it is not unified? How can the canopy gaps distribution/orientation (to south or north and to zenith or horizon) be considered?

We assumed that there are some preferred directions because the solar radiation is coming with varying intensity depending on the direction. Thus we need to count in the distribution of canopy gaps over the hemisphere and to consider the orientation of the canopy gaps. Therefore the set of three basic characteristics, calculated for the entire view, was extended by adding derived characteristics for limited view/azimuth angle and zenith angle. Each canopy characteristic was calculated for 3 zenith angles - 30, 60 and 90 degree, and for 4 aspects/ azimuth sections – north (N), east (E), south (S), west (W), and entire view. It means 45 characteristics of canopy per point.

CCL is simply calculated as a ratio of number of black pixels representing canopy to number of all pixels representing entire view. This calculation is conducted out of Hemisfer software. While the CCL and transmission calculation is quite straightforward, the transmission and LAI estimation is more complex because several additional factors coming into play in calculation. It brings the higher variability of methods and algorithms to obtain LAI value. There are implemented all commonly used algorithms of LAI calculation in Hemisfer (Figure 2.1) because it was developed to compare those methods (Thimonier et al. 2010).

The apparent leaf area, which obscures the sky, depends on the leaf angle. The ratio between the apparent area of a leaf and its real area is the projection coefficient G. It is a function of the leaf zenith angle Θ (theta) and the leaf inclination α (alpha). Because not all leaves have the same inclination angle, their statistical distribution has to be taken into account when estimating the LAI.

Schleppi et al. (2007) describes the basic process of transmission and LAI calculations in Hemisfer software. The (light) transmission is calculated in the Hemisfer software as the proportion of white pixels within analysis rings, i.e. as a discrete function of the zenith angle Θ (theta). The next step is to calculate the contact number $K = -\cos \Theta \ln T$. K is the average number of times that a light ray would touch the canopy when travelling a distance equal to the thickness of the canopy T. Then the K values are finally integrated over the rings to give the LAI, but this step differs among methods:

Miller (1967) method is based on assumption that the effect of the leaf angle disappears when integrated over all viewing angles of the hemisphere.

Li-Cor LAI-2000 canopy analyzer uses slightly modified Miller (1967) method. The both methods are equal for the entire view (LI-COR Inc. 1992).

Lang (1987) proposed to estimate the value of K at 1 rad by a linear regression against Θ, because K values are almost unaffected by the leaf angle for the zenith angle of $\Theta = 57° = 1$ rad.

Norman et Campbell (1989) algorithm uses a least square method and ellipsoidal model of leaf angle distribution to estimate jointly the LAI and the leaf angle, which are related to each other.

Weighted ellipsoidal method (Thimonier et al. 2010) optimized the previous method.

Hemisfer software offers also further corrections: non-linearity correction (Schleppi et al. 2007), canopy clumping correction (Chen etCihlar 1995), slope correction (Walter et Torquebiau 2000), or clumping correction (Lang & Xiang

1986). Any of the corrections can be applied to any of the methods. No corrections were used in present study in order to keep the calculation simple.

For the review of methods see (Thimonier et al. 2010).

LAI estimation is easier with assumption that the leaves are randomly distributed within the canopy and tends to fill the gaps. Unfortunately this assumption is often not valid in case of mountain coniferous forests, where the canopy is clumped to better withstand snowy conditions. More light reach the ground in a clumped canopy than in random canopy because leaves are hiding each other and leave larger gaps in between. Therefore the LAI derived from transmission, called effective LAI (LAIe), is lower than real LAI. Nilson (1971) defines clumping index Ω (omega) as LAIe/LAI. Clumping is the tree strategy to reduce interception and the snow under the canopy is affected by total radiation reaching the ground. Thus the snow distribution should be related more to LAIe than LAI. Therefore we considered LAI = LAIe in present study.

LAI by (Miller 1967) was selected for calculations within this study. This method is the classic one but the method selection is not crucial for this study results, because the cross correlation test conducted on the set of 112 hemispherical pictures from the research sites confirmed high correlation among all methods.

3.8 Manual canopy classification

A simple manual classification was proposed as an alternative method for a quick evaluation of canopy characteristics as compared to the typically time consumptive HP process. The classes were designed so that they capture information about canopy density, shading from the south and drop-off zones. Figure 3.5 shows the set of 6 classes which were utilized.

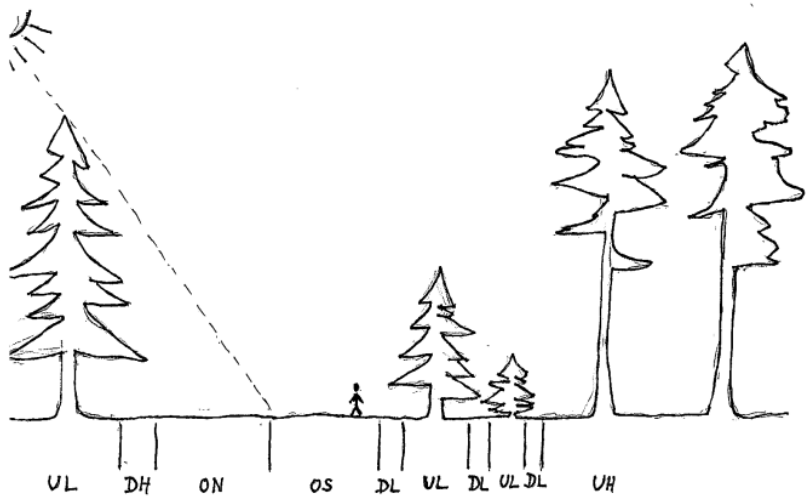

Figure 3.5: Manual canopy classification into 6 categories: Open to the sun/south (OS), Open to the north (ON), Under the tree with high branches (UH), Under the tree with low branches (UL), Drop-off zone of high tree (DH), Drop-off zone of low tree (DL)

It would be always possible to add more and more classes to get better situation description because there is continuous spectrum of differences. But on the other hand the classification system should be as simple as possible. Therefore the 6 classes system was proposed, tested and finally used for assessment of experimental sites.

3.8.1 Classes description

OS – open to the south or open to the sun

The point is not under canopy. It is part of some (small or large) open area. We can see large part of the sky from this point, if we look up staying at this point. The south part of the sky is visible and so direct solar radiation can access the point.

ON – open to north or open and no sun

The point is not under canopy. It is part of some (small or large) open area. We can see large part of the sky from this point, if we look up staying at this point. But the south part of the sky is not visible and so direct solar radiation can't access the point. The point remains in shadow.

UH – Under the tree with high branches

The point is under canopy of a high tree. Branches are more than 3 m above the ground at the point.

UL – Under the tree with low branches

The point is under canopy of a tree with low branches. It does not matter whether the tree is high or low. Branches are less than 3 m above the ground at the point.

DL – Drop-off zone of low tree

The point is under canopy of young low tree – maximal height about 8-10 m. The point is under end of the lowest branches. And so we can expect that the snow sliding down the branches would reach the point.

DH – Drop-off zone of high tree

The point is under canopy of high tree (more than 8-10 m) with low branches. The point is under end of the lowest branches. And so we can expect that the snow sliding down the branches would reach the point. This class is similar to DL class, but higher tree has more branches above the point and so more dropped-off snow is expected at the point.

Only the drop-off zones of the trees with low branches are captured by this classification because the drop-off from high branches is scattering in large area.

The drop-off zones are restricted only on the (small or high) trees with low branches. Low branches cause the concentration of the snow sliding down from the tree to the small area. If the tree has no low branches, the wind causes random scattering of dropped-off snow in large area and no clear drop-off zone can be determined. There are two separate drop-off zone classes for small and high trees with low branches, because the tree height has influence on the amount of (precipitated and subsequently) dropped-off snow.

3.8.2 Additional information

The classification of spot conditions is not always absolutely clear. Therefore the certainty level was used: 1 for clear cases, 2 in case of some doubts and 3 for ambiguous situations (1 is default value, which has not to be explicitly written).

If there are any very special conditions at the spot, it is described in separated and numbered comment. Special conditions could be dry trunk, stump, fallen tree, etc.

It was considered as useful to record the combined class like DH-OS for some spots. But always the first class indicates the dominant influence. The second is less important additional information.

3.8.3 MCC Testing

Manual canopy classification is obviously prone to some subjectivity and dependency on observer-evaluator. The objectivity of the classification was tested to estimate the influence of subjective observer evaluation and stability to change of observer-evaluator. A small group of testers independently evaluated the same area with variable canopy structure after reading the guidelines for manual canopy classification (where detailed description of all classes is provided). Three testers classified the canopy at all 276 points of one site. Drusatscha medium site was chosen because of high variability of canopy structure.

	OS1	OS2	OS3	ON1	ON2	ON3	UL1	UL2	UL3	UH1	UH2	UH3	DL1	DL2	DL3	DH1	DH2	DH3
OS1	1	0.9	0.8	0.5	0.7	0.7	0	0.1	0.2	0.2	0.3	0.3	0	0.1	0.2	0	0.1	0.3
OS2	0.9	1	0.9	0.7	0.8	0.7	0.1	0.1	0.2	0.3	0.3	0.4	0.1	0.1	0.2	0.1	0.2	0.3
OS3	0.8	0.9	1	0.7	0.7	0.8	0.2	0.2	0.2	0.3	0.4	0.4	0.2	0.2	0.2	0.3	0.3	0.4
ON1	0.5	0.7	0.7	1	0.9	0.8	0	0.1	0.2	0.2	0.3	0.3	0	0.1	0.2	0	0.1	0.3
ON2	0.7	0.8	0.7	0.9	1	0.9	0.1	0.1	0.2	0.3	0.3	0.4	0.1	0.1	0.2	0.1	0.2	0.3
ON3	0.7	0.7	0.8	0.8	0.9	1	0.2	0.2	0.2	0.3	0.4	0.4	0.2	0.2	0.2	0.3	0.3	0.4
UL1	0	0.1	0.2	0	0.1	0.2	1	0.9	0.8	0.4	0.5	0.6	0	0.2	0.3	0	0.2	0.3
UL2	0.1	0.1	0.2	0.1	0.1	0.2	0.9	1	0.9	0.5	0.6	0.7	0.2	0.3	0.5	0.2	0.3	0.5
UL3	0.2	0.2	0.2	0.2	0.2	0.2	0.8	0.9	1	0.6	0.7	0.8	0.3	0.5	0.6	0.3	0.5	0.6
UH1	0.2	0.3	0.3	0.2	0.3	0.3	0.4	0.5	0.6	1	0.9	0.8	0	0.2	0.3	0.2	0.3	0.3
UH2	0.3	0.3	0.4	0.3	0.3	0.4	0.5	0.6	0.7	0.9	1	0.9	0.2	0.3	0.5	0.3	0.3	0.4
UH3	0.3	0.4	0.4	0.3	0.4	0.4	0.6	0.7	0.8	0.8	0.9	1	0.3	0.5	0.6	0.3	0.4	0.4
DL1	0	0.1	0.2	0	0.1	0.2	0	0.2	0.3	0	0.2	0.3	1	0.9	0.8	0.5	0.6	0.7
DL2	0.1	0.1	0.2	0.1	0.1	0.2	0.2	0.3	0.5	0.2	0.3	0.5	0.9	1	0.9	0.6	0.7	0.7
DL3	0.2	0.2	0.2	0.2	0.2	0.2	0.3	0.5	0.6	0.3	0.5	0.6	0.8	0.9	1	0.7	0.7	0.8
DH1	0	0.1	0.3	0	0.1	0.3	0	0.2	0.3	0.2	0.3	0.3	0.5	0.6	0.7	1	0.9	0.8
DH2	0.1	0.2	0.3	0.1	0.2	0.3	0.2	0.3	0.5	0.3	0.3	0.4	0.6	0.7	0.7	0.9	1	0.9
DH3	0.3	0.3	0.4	0.3	0.3	0.4	0.3	0.5	0.6	0.3	0.4	0.4	0.7	0.7	0.8	0.8	0.9	1

Table 3.2. The evaluation matrix used to compare assessment obtained by different observers

The results were compared to check the correlation between independent observers. The correlation was evaluated for each point and each pair of observers. Then the mean correlation value was calculated as the measure of objectivity and independency on observer. The correlation between the canopy classes cannot be exactly calculated. Therefore the evaluation matrix setting up the approximate

correlation was proposed and used for assessment. The matrix contains pairwise correlations for all possible manual canopy classifications as in Table 3.2. Pairwise correlations reflect the similarity between the classes.

After this testing, the manual classification was carried out by a single observer for all measuring points at all field sites.

3.9 Aerial laser scanning

3.9.1 Data

Two airborne LiDAR data sets, with average rasterized resolutions of 0.5 m (Figure 3.6) respectively 2 m, were employed in the canopy structure analysis. The fine data set was available for an area of 90 km^2 including the research sites and the coarse one was available for whole Switzerland. Data were acquired by a series of helicopter flyovers at a nominal flying altitude of 700 m using a Riegl LMS-Q560 sensor. This device emitted 1550 nm wavelength light in 5ns pulses and recorded up to 7 returns per pulse within view angle of ±15°. The affiliated DTM were computed by using the classified ground returns at a 0.5 m horizontal resolution by Toposys using their in house processing software, TopPit. (TopoSys 2015, Moeser et al. 2015)

Swisstopo, Swiss Federal Office of Topography, provides the national LiDAR dataset –DSM with pixel size of 2 m and the altimetric precision (simple standard deviation) on unspecified place is better than ± 1.5 m. (SwissTopo 2013). These data are publicly available to download. There are already even higher resolution datasets available in few other European countries like Sweden, and the situation with data availability is getting even better every year.

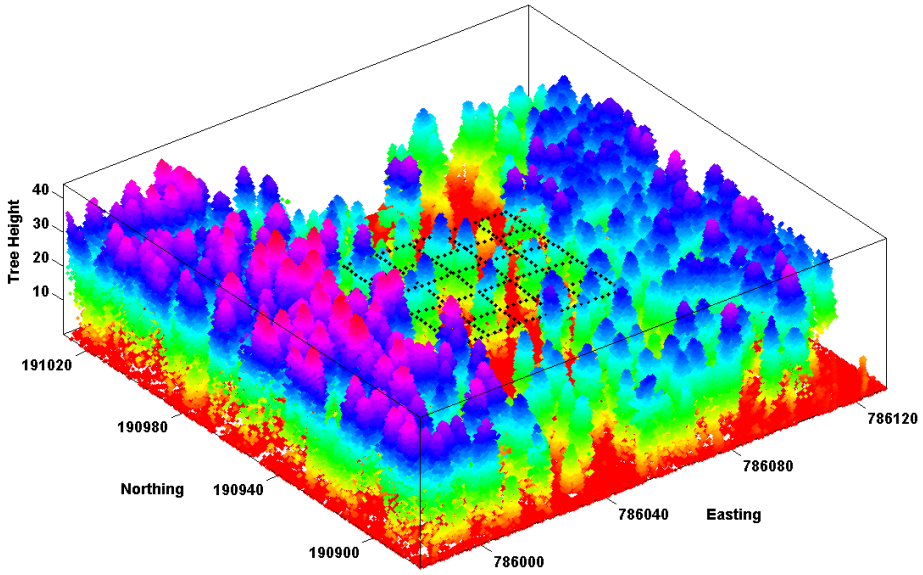

Figure 3.6: LiDAR cloud data of the Laret low field site. The geo-rectified sampling grid is the internal black dotted line and is 50m by 50m.

3.9.2 Cartesian approach processing

CCL was calculated from raw LiDAR data by converting all returns from the point cloud into a 0.5 m grid and then quantifying the ratio of cells which have canopy cover to the total number of cells within the digital surface model (Moeser et al. 2014). LAI values were computed as the ratio of all raw LiDAR first returns to total ground returns and was derived from a modified routine initially utilized by Morsdorf et al. (2006). This approach is called Cartesian after the coordinate system used in calculations. Dislike the hemispherical photography which observes the world in spherical coordinates. The height cutoff of 1.2 m, corresponding with HP cutoff caused by the tripod height, was used.

The result of Cartesian method depends on the size of considered buffer area around the point. The sensitivity to the size change was studied in order to find the optimal area size. The box size was varied from 0.5 to 100m with the step increasing with size. CCL was calculated for distinct view angles (30°, 60° and 90°). While the LAI values were always calculated for the entire viewshed.

3.9.3 Synthetic hemispherical photos

LiDAR data provides information about canopy spatial distribution in the form of point cloud. This information can be used to create artificial/synthetic hemispherical photos (AHP) by the way of visualization of this point cloud using angular approach to show what is visible from selected point on the ground.

AHP creation process starts with point cloud transformation from the Cartesian XYZ coordinates to spherical/polar ΘΦR coordinates with the center in selected point on the ground, resp. at height 1.2 m above the ground equal to the hemispherical camera tripod height. The second step is to visualize these points in the picture. The position of the point image in the synthetic picture is determined by zenith and azimuth angle (Θ and Φ). Size of the pixel visualizing the point in the synthetic picture is a function of distance (R) from the origin. Sensitivity analysis was conducted to select the best function from proposed set of candidate functions consisting of several constants and linear functions R or vertical distance (R*sin Θ).

For the AHP sensitivity analysis result and for AHP canopy characteristics comparison to real HP see the section 4.8; for more details about data preprocessing see (Moeser et al. 2014).

3.10 Hemispherical photo processing

The hemispherical pictures were processed in a hemispherical photo processing software package, Hemisfer (Schleppi et al. 2010; Thimonier et al. 2010) to arrive at canopy characteristics. The Hemisfer software provides many different characteristics: LAI according to several methods for whole scene and per sectors (for limited azimuth angle), transmission and number of white and black pixels for scene or per sector and ring (for limited zenith view angle). All canopy characteristics calculations in Hemisfer are based on the classification of pixels to either white (=sky) or black (=canopy) by applying a brightness threshold to the

analyzed picture. The new version 2 beta of Hemisfer was tested. This version provided also calculation of light regime (potential incoming solar radiation).

LAI and CCL were used for analysis in this study. LAI was calculated by the guidelines outlined by Miller (1967). CCL values were calculated from looking at the ratio of white to black pixels. The choice of another LAI calculation method would not have big influence on results, because the correlation of values obtained by Millers method to values obtained by other methods (for 112 pictures taken at research sites) is very high (0.93 - 1.00).

Following setup of Hemisfer software was used: lens – Sigma 4.5, threshold – 81, division of the view-shed into 6 rings and 4 sectors, north at azimuth 180.5 (according to the north arrow in pictures). Especially threshold setting is very important because all methods used in Hemisfer are based on the classification of pixels to either white (sky) or black (canopy). For less contrast pictures the lower threshold value was used and color settings were changed to make blue and light colours more probably to evaluate as the sky and green and dark tones as the canopy. The setup of locality with coordinates is important for light regime calculations in Hemisfer version 2.

All Hemisfer canopy characteristics result files were transformed by Python script, because the original result file structure is quite complicated for automated reading by Matlab and Python is more flexible in text file processing than Matlab. Transformed file structure is simple table in tab separated value text format, where each row represents one point and each column contains values of one parameter. It is easy to read the data from restructured files in Matlab, which was used for all data analysis.

Light regime result files provided by Hemisfer 2 beta has more convenient and simplier structure. These files can be easy read directly by Matlab. (Hemisfer 2beta provides also light regime result file, which has more simple structure and can be easy read directly in Matlab.)

3.11 Hemispherical photo analysis

The alternative methods to get the canopy characteristics were compared to the (real) hemispherical photography method, which is considered as the reliable reference method.

(1) Dependency of correlation of Cartesian LiDAR based canopy characteristics and HP canopy characteristics on bounding box size was studied for following canopy characteristics: CCL values for the different view angles (30°, 60° and 90°) and LAI for the entire viewshed. Correlation coefficient maximum was used as the criterion for finding the optimal box size with the best match of values with values obtained from hemispherical pictures (see section 4.7).

(2) LAI and CCL obtained from real and synthetic hemispherical pictures were compared. Correlation coefficient and normalized root mean square error was calculated to evaluate the expected dependency. (See section 4.8)

(3) Manual canopy classification was not directly compared to HP, because each of these methods provides different type of result. HP provides exact numerical

indexes (from continuous interval) and manual canopy classification provides descriptive canopy class (from the discrete set). Both of the results were compared to snow cover data Correlation analysis was used for continuous quantitative indexes and snow data (see sections 4.4 and 4.9) and the differences in snow data between different qualitative classes were studied (see 4.4).

3.12 Snow data analysis

Basic overview and summary of measured snow data for whole season 2012/13 was done as the first step. Basic statistics was calculated. Measured data was organized into datasets for forest HS and SWE and for open HSo and SWEo for all campaigns and new (sometimes called differential or storm HS) HN for only subset of campaigns.

Relative snow depth (rHS) data set was derived from forest HS and open HSo. Relative HS in forest is the ratio of forest HS to mean HS at related open area:

(3.12-1) $rHS = HS/HSo$

New snow depth (HN) is the depth of new snow from the last snow storm. This value is not available for all campaigns.

The courses of snow depth, relative snow depth and SWE during the season were analyzed to identify accumulation and ablation period. Average values per site and global average values were calculated to identify the date of maximum snow accumulation. This date was used as the end of accumulation period

Following analysis were focused on relationship between HS and canopy characteristics. (SWE data was not included in these analyses because of limited extend of this study):

- **HS and HP based canopy characteristics**

The relation between HS and real HP derived CCL or LAI was analyzed for the set of 112 points (all 16 inner poles per each of all 7 sites). Correlations were calculated and contour plots were used to visualize the relationship and its changes during the season.

- **HS and synthetic HP based canopy characteristics**

The same analysis was performed also for canopy characteristics derived from synthetic LiDAR based hemispherical pictures. The same 112 point set was analyzed first. And then the analysis was run for the set of all points for all sites (276 points for each of 7 sites).

- **HS and canopy classes**

Another option how to compare HS to canopy properties for all points is to use manual classification data for canopy. HS, relative HS and new snow depth data series for each canopy class were calculated and inter-compared to investigate the influence of canopy class on snow cover. The seasonal course and its variability with canopy category was studied.

3.13 Snow model

A model for snow cover under forest canopy expresses the amount of snow (HS, SWE) as a function of canopy characteristics and the amount of snow in an open area (3.13-1).

$$HS_f = f_{HS}(\{CN_i, i=1..m\}, \{SC_{o\,i}, i=1..n\}) \quad (3.13\text{-}1)$$

Where HS_f is snow depth at a given point in the forest, $\{CN_i\}$ is a set of m parameters describing canopy cover at that point (selected canopy cover characteristics) and $\{SC_{oi}\}$ is a set of n parameters describing the snow cover in an open area.

The snow height was used as the snow amount measure in models in this study. Similar analysis and models could be performed for SWE too. They are not included in this thesis because of limited time and page extend.

The expression (1) is very general. Searching a specific form of the expression is the modeling process or process of model building. This process could be pure statistical or some physical relations could be embedded. Following sections describe the model building process.

3.13.1 Snow predictor search

The model building process consists of the identification of model parameters and the determination of the functional relation between modeled variable and model parameters. The best snow predictor among the canopy characteristics was searched.

Investigation of the relationships between snow and canopy characteristics was based on statistical analysis. The first step in this process was the definition of a set of canopy characteristics as potential snow predictors. This set covers a large amount of variables for global view or view limited by zenith or azimuth angle (canopy closure, canopy closure to the south, north, east, west, 120 degree canopy closure etc.).

Correlation of those parameters with snow cover characteristics was analyzed to determine the most powerful predictors. Good predictors should be highly correlated to predicted property – snow amount. The highest correlated characteristic was selected as the first member of predictor set. The intercorrelation and linear dependency among the characteristics must be taken into account for the selection of the second predictor into the set.

Principal component analysis (PCA) and k-means clustering was used to split the set of potential predictors into clusters based on linear dependency. The original set of potential predictors contains linearly dependent variables. This large set of variables was reduced to a tiny set of predictors using 2 requirements: high correlation to predicted variable (amount of snow) and linear independence of the set. Linear independence helps to reduce the dimension of the predictor set and keep the dimension of space generated by them. PCA is a multivariate statistical method usually used to identify the main components (eigenvectors) and to use them as the orthogonal base. In this case the main components were not used because they don't

have such a clear physical meaning as the original variables. The final set of predictors is used as the set of input parameters in the model. The model parameters should have a clear physical meaning. They should be linearly independent but not necessarily orthogonal.

After setting up the model parameter set, the generalized linear model (GLM) was used to resolve the functional relation between modeled property (dependent variable) and input model parameters (independent variables). Two different models of the amount of snow under the canopy were established and subsequently compared: statistical model and a physical based model

3.13.2 Statistical model

The statistical model was formulated as the direct relationship between snow height and the canopy described by (selected) canopy characteristics and the snow height in an open site.

The expression (3.13-1) was rewritten as

(3.13.2-2) HSf = HSo * rHS

Where rHS is relative snow height (relative to the open site)

(3.13.2-3) rHS = HSf / HSo = frHS({CNi, i=1,2})

There is a significant difference in canopy influence on snow during accumulation and during ablation. Therefore the model was divided into 2 separately calculated parts for accumulation and for the depletion period. For each period, the model was set up using equations (3.13.2-2) and (3.13.2-3). Function frHS was modeled as GLM with 2 independent parameters - 2 selected canopy characteristics.

3.13.2 Physical based model

The physical based model was set up as a more complex alternative to the simple statistical model. As there are many physical factors influencing snow cover, there are also many ways of how to set up the physical model. The more physical processes and quantities are considered, the more complicated the model structure becomes and the more input parameters are needed. But often there are no available detailed measurements of temperatures, heat fluxes, radiation, run off, evaporation etc. Therefore our model was kept simple to reduce input data requirements.

The model does not require any direct measurement of meteorological conditions. No influence of meteorological conditions is explicitly expressed in the model. The response of snow cover to changing meteorological conditions is implicitly hidden in snow data for the open site.

The model is based on a mass balance equation (3.13.3-1) quantifying the mass balance processes caused by canopy.

(3.13.3-1) $HS_f = HS_o - I + DO + DD$

Where HSf is snow depth at a given point in the forest, HSo is snow depth in an open area, I is canopy interception, DO is snow drop-off from canopy and DD is the depletion difference between the forest and the open site.

Accumulation of snow under the canopy consists of through fall which is reduced by interception and amplified by drop-off. Canopy shield reduces the depletion. According to the equation (3.13.3-1), the model is decomposed into 3 parts modeling these 3 processes.

(3.13.3-2) $f_{HS} = HS_o - f_I(\{CN_i\}, HS_o) + f_{DO}(CN_M, \{CN_i\}, HS_o) + f_{DD}(\{CN_i\}, rHS_o, HS_{fmax})$

Where CN_M is the canopy manual classification, $\{CN_i\}$ is a set of canopy characteristics, HS_o resp. HS_f is snow height in the open resp. forested area, HS_{fmax} is the maximal seasonal snow height and rHS_o is the relative (percentage of the maximum) snow height in the open site.

Interception model

Interception was calculated as the difference between new snow height in the open and under the canopy in the forest.

(3.13.2-3) I = HSo – HSf

The model does not work with absolute interception I, but with relative interception rate IR.

(3.13.2-4) IR = I / HNo = (HNo – HNf) / HNo = 1 – HNf/HNo

Interception rate is modeled as a function of selected canopy characteristics. Canopy characteristics used in this case are T-30 and LAI. This function was searched as GLM (linear regression in this case).

(3.13.2-5) IR = fIR($\{CN_i\}$) = fIR (CCL30,LAI) = b0 + b1*CCL30 + b2*LAI

Interception was used in the model of snow height out of drop-off zones.

(3.13.2-6) Hs = HSo – I =HSo (1 – IR)

The equation (3.13.2-6) uses total snow heights instead of new snow heights. The total amount of snow is reduced by the same interception rate as each new amount of snow.

(3.13.2-7) (1 – IR) = HNf / HNo = HSf / HSo

This assumption comes from the following deduction. Total snow height is the sum of new snow heights reduced by settling.

(3.13.2-8) HS = ∑HNi*SRi,where NNi and SRi are new snow height and the settling rate for each snowpack layer.

Using (3.13.2-8) and (3.13.2-8) we get (3.13.2-9) which is equal to (3.13.2-7):

(3.13.2-9) HSf = ∑HNfi*SRi = ∑(1-IR)*HNoi*SRi = (1-IR)*∑HNoi*SRi = (1-IR) * HSo

New snow data were used for the interception model calibration. The advantage is that all points including drop-off zones can be used for calibration by new snow data because new snow height is not influenced by drop-off.

The interception model can be used to calculate total snow heights only out of drop-off zones during the accumulation period.

Drop-off model

The drop-off model was developed to calculate the amount of snow inside drop-off zones (DOZ) during the accumulation period.

The key question was how to calibrate the drop-off model if there were no direct drop-off measurements. The only available data are total HS (and SWE) lacking any information how much is the drop-off contribution. But on the other hand the main purpose of the drop-off model is the calculation of total HS in DOZ, where the pure interception model is not useful.

Therefore the grid was split into 2 parts: DOZ and ZOD (zones out of drop-off). The decision criterion was the value of manual canopy classification because of 2 reasons: 1) there is no straight relation between any canopy characteristic and drop-off zone and 2) manual canopy classification (dislike the real HP images) is available for all grid points.

The model works with relative snow height (relative to the open site) rHS:

(3.13.2-10) rHS = HSf / HSo = frHS({CNi, i=1,2})

It assumes that rHS is a function of canopy characteristics. Canopy characteristics used in this case are canopy closure for limited 30° zenith angle and LAI. The function was searched as GLM (linear regression in this case).

(3.13.2-11) rHS = frHS({CNi}) = frHS (CCL30,LAI) = b0 + b1*CCL30 + b2*LAI

After the calibration the vector b is known and HS is calculated from HS in the open area and canopy characteristics at the point:

(3.13.2-12) HSf = HSo * frHS(CCL30,LAI)

Depletion model

The depletion model quantifies the snow depletion during the depletion period. If there is any depletion during the accumulation period, available measurements do not allow to separate it from other processes. Anyway, accumulative processes are strongly dominant during the accumulation period in mountainous areas because of the relative high altitudes and cold temperatures.

Depletion was defined as the difference of maximal HS and actual HS (3.13.2-13) and modeled as the function f_{DD} (3.13.2-14) of canopy characteristics {CNi}, snow height in the open site HSo and maximal snow height in the open site HSomax. The last two variables were used in the form of a ratio as rHSo is relative snow height in the open site (relative to the maximum). GLM model (nonlinear regression) was used for f_{DD} function approximation.

(3.13.2-13) DD = HSfmax -HSf

(3.13.2-14) DD = f_{DD}({CNi} $_{i=1,2}$, HSo/HSomax, {CNi*rHSo} $_{i=1,2}$)

CCL90S was selected because it reflects canopy openness to the south. Strong influence of direct solar radiation coming from the south direction was expected.

The f_{DD} function can sometimes return small negative HSf in case of a very low HSo. All negative values are replaced by zero.

Composed model

The physical based model of snow height in the forest HSf was set up as the composition of the interception, drop-off and depletion models. This model uses the algorithm which decides if it is accumulation or depletion period and if the point is in the drop-off zone or not. The algorithm applies a proper model according to the situation. Input data for the model are: HS in the open site, canopy characteristics (CCL30, LAI, CCL90S and manual canopy classification - DOZ).

There are two additional input parameters necessary in the depletion part of the model: HSomax - maximal HS in the open site and HSfmax – maximal HS at the point in the forest. HSomax is easily obtained as a maximum of HSo. HSfmax could be either another input parameter, if it is available from measurement (as in this case), or it must be calculated using the accumulation part of the model and subsequently used in the depletion model.

Another important model parameter is switching the point between accumulation and depletion. The model uses the time of maximal accumulation in the open site. The switching point can be a bit shifted for forested sites. But this time difference is usually short enough to be neglected. In this case the maximum accumulation time was in time of 6^{th} campaign for all open and forested sites except for Laret high, where the maximum was reached one campaign later.

The significant difference in the timing of maximal accumulation was observed for SWE. The peak of SWE was 2 campaigns (about 20 days) later than the HS peak. Shifting the switching point a bit later would not bring any problems, because the difference between the depletion and accumulation model is small for the very beginning of the depletion period. The model is quite stable and not very sensitive to this shift.

4 Results and Discussion

Figure 4.1 shows the scheme of the results. The structure is divided into data acquisition and processing (blueish entities), data analysis and modeling (reddish). The gray part represents the related project parts, which are not (or not completely) covered by this study. The chart clarifies the results structure and linkage among its components, even if the reality does not allow us to draw such an exact border line between the entangled components of the chart. Therefore each section of this chapter deals with a cluster of the linked components.

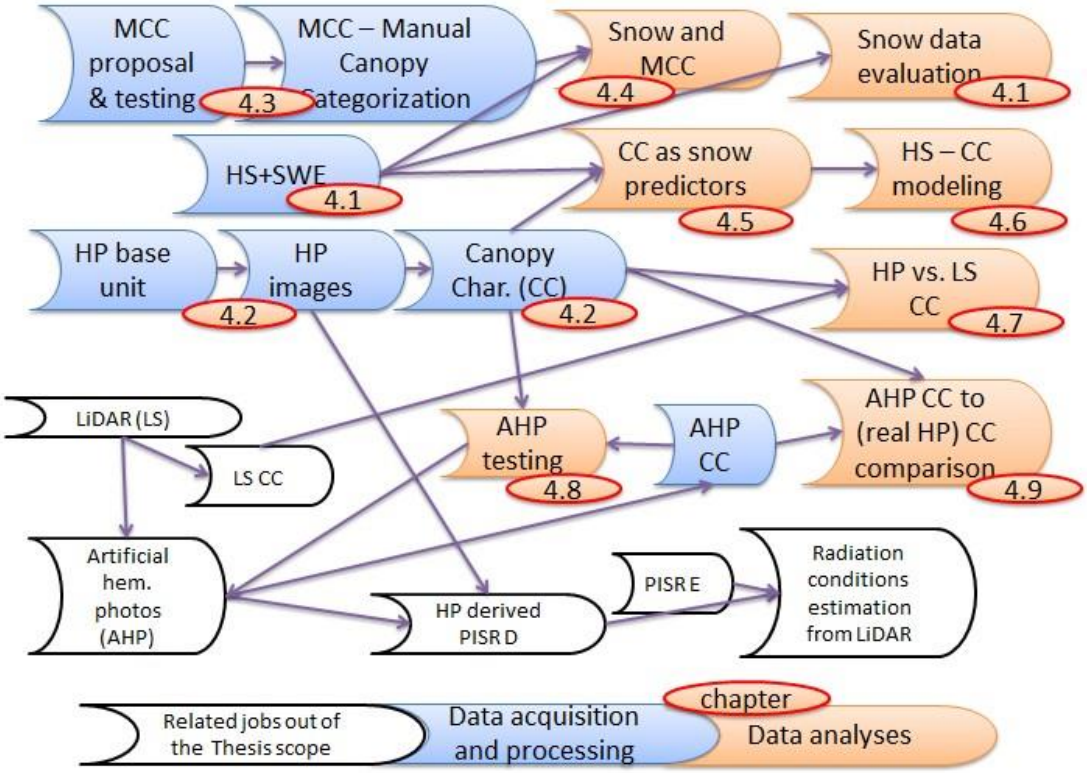

Figure 4.1: Project result scheme

4.1 Snow cover characteristics

Large database of snow data was built up during the entire winter season 2012/2013. The database consists of nearly 40000 single measurements (approximately 30000 HS, 8000 HN and 1000 SWE measurements). During the accumulation period up until the end of February, 6 campaigns were conducted. Maximum snow accumulation was reached on the 21st February at open sites. Subsequent ablation period lasted until the end of April and was covered by another 9 campaigns. Because of the limited extent, this study focuses primarily on HS analysis.

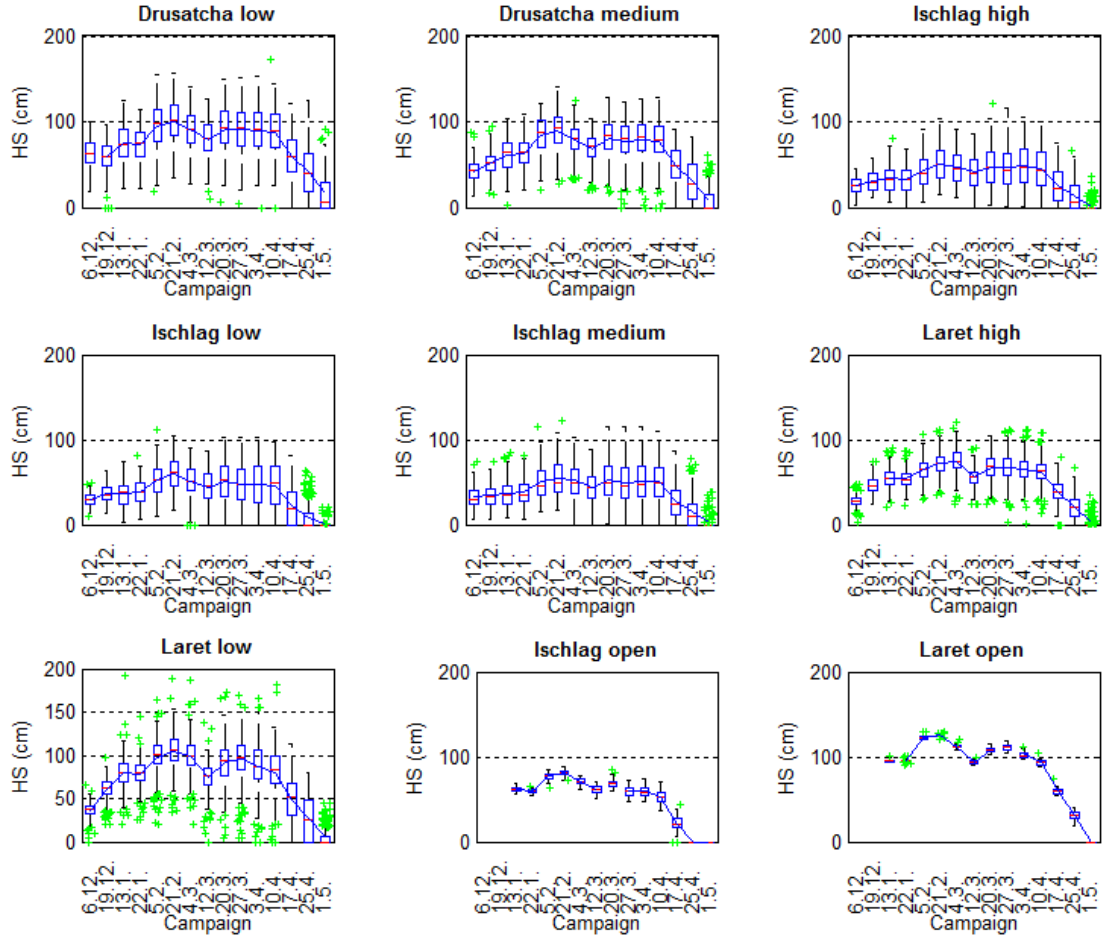

Figure 4.2: Variability of HS per site during the season. Line stays for mean HS.

The exact maximum accumulation time varied only very slightly with the elevation and the canopy density, the differences were smaller than the time resolution of campaigns. Only at the Laret high site, the delayed maximum due to high canopy density was observed. The snow cover duration also varied with the canopy structure and elevation. Not only canopy density but also the aspect of canopy gaps played a significant role in ablation. (This is shown in Figure 4.8.) Against the expectation the measurement does not proved increase in HS with increasing elevation. The observed trend was reversed, which could be due to wind transport from strongly wind exposed high elevated parts to lee sites further down.

The wind transports the snow from higher areas with higher wind speed down to the valley, where the wind slows down and its transport capacity therefore diminishes.

The ablation period was interrupted by another short but significant accumulation sub-period at its beginning between 12th and 20th March. The depletion rate has an increasing trend during the ablation period, which could be easy described by increasing solar energy input. Lower depletion rate was observed also under the denser canopy because of higher shading reducing the solar energy input.

Much less spatial variability of HS open at any time during the season is obvious from the Figure 4.2. The higher forest density sites exhibit lower spatial HS variability, which could be explained by lower spatial variability of canopy density. This effect is clearly visible particularly for the Laret and Drusatcha sites.

4.2 Hemispherical photography and canopy classification

The overview of the canopy structure variability within the sites and among them is given in Figure 4.3. The first two plots shows LAI and CCL for the entire hemisphere while the other two represents CCL for limited zenith and azimuth angle. Even if some correlation between CCL and LAI mean values is visible, the variability of LAI exhibits a different behavour than the CCL. The highest variability of the LAI was observed together with relative low variability of the CCL at the Ischlag high site. The limited zenith or azimuth angle brings higher variability. Although each of them in different manner.

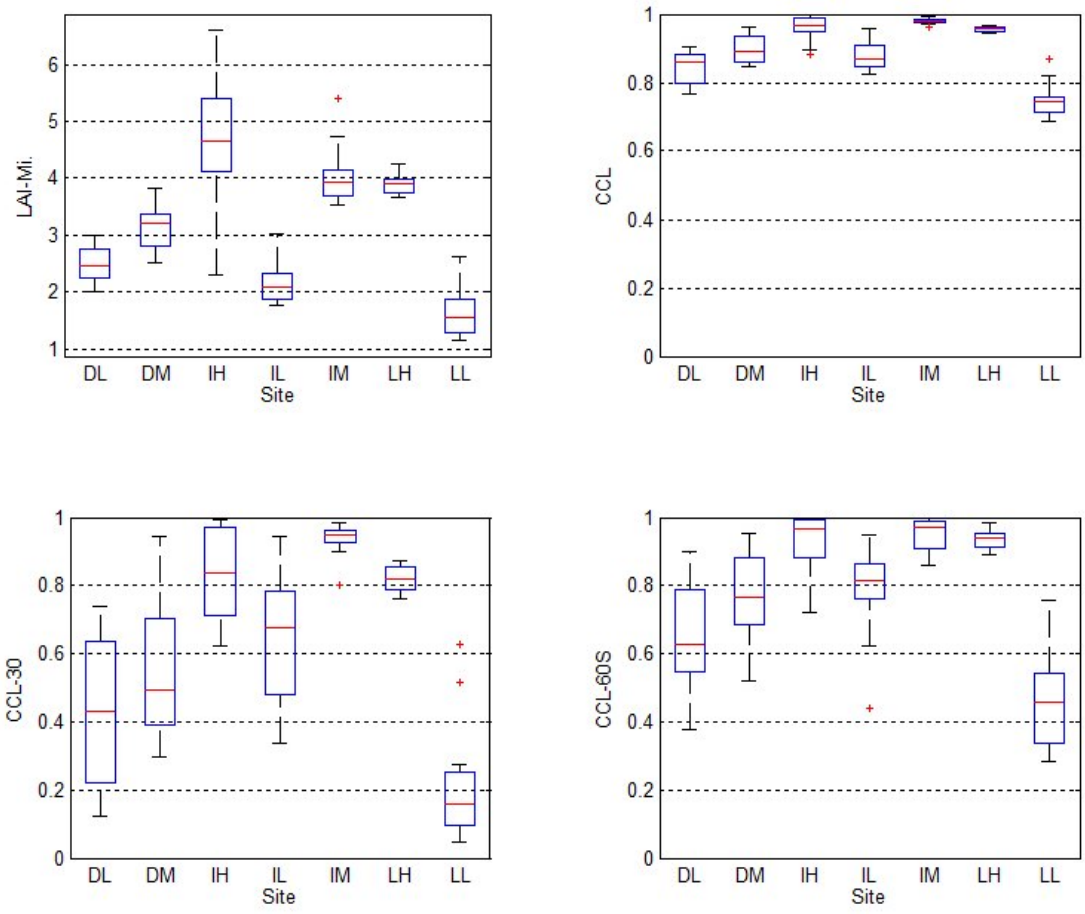

Figure 4.3: Comparison of site canopies using HP derived LAI, CCL and CCL for restricted zenith view

The canopy characteristics were derived from (real) hemispherical pictures taken at all sites. Figure 4.4 illustrates the canopy at the sites showing selected HP images. Even if only 4 images per site are presented, they represent well the site conditions, shown also in the previous Figure 4.3. It also reveals the fact that the site name suffix (high, low, medium) is good to distinguish between the sites locally, but not to describe canopy density globally. At the raw images, we can see that even if we did our best, the light conditions were not always perfect. Therefore some color corrections were necessary for accurate image classification.

No clumping corrections were applied in LAI calculations in the present study to keep it simple. The relative comparison among the points was more important than absolute accuracy anyway. If the highest accuracy of absolute LAI values would be required then knowledge of clumping index could help to get better results for coniferous stands.

The necessary preconditioner result for taking HP pictures was the design of the HP base unit for conversion between the tripod and the hemispherical camera, which is described above in the section 3.6. The result of designing process, the base unit proved to be very effective during the fieldwork. When we were hiking up to sites, we appreciated how light it was. On the other hand it was robust and easy to use. No change requirement did appear during the field measurement.

4.3 Manual canopy categorization

The method of quick canopy assessment by manual categorization was proposed and described in the section 3.8. This set of classes was optimized to capture the canopy influence on snow cover. Therefore it reflects the light regime (openness to the south) and precipitation regime (drop-off zones) at the spot. Even if these factors are important in general, the usage of manual classification for other purpose in forest research is probably limited and would require some modification in the scale.

The test of the method objectivity (described in the section 3.8.3) resulted in mean pairwise correlation value 0.77. Thus means there the significant differences between categorization done by different observers are not frequent. The evaluators assigned usually a single category to each point. The alternative option to add the second alternative category was used rarely, in less than 4% cases. The certainty level 3 was not used at all. And the certainty level 2 was used in 19% of evaluations.

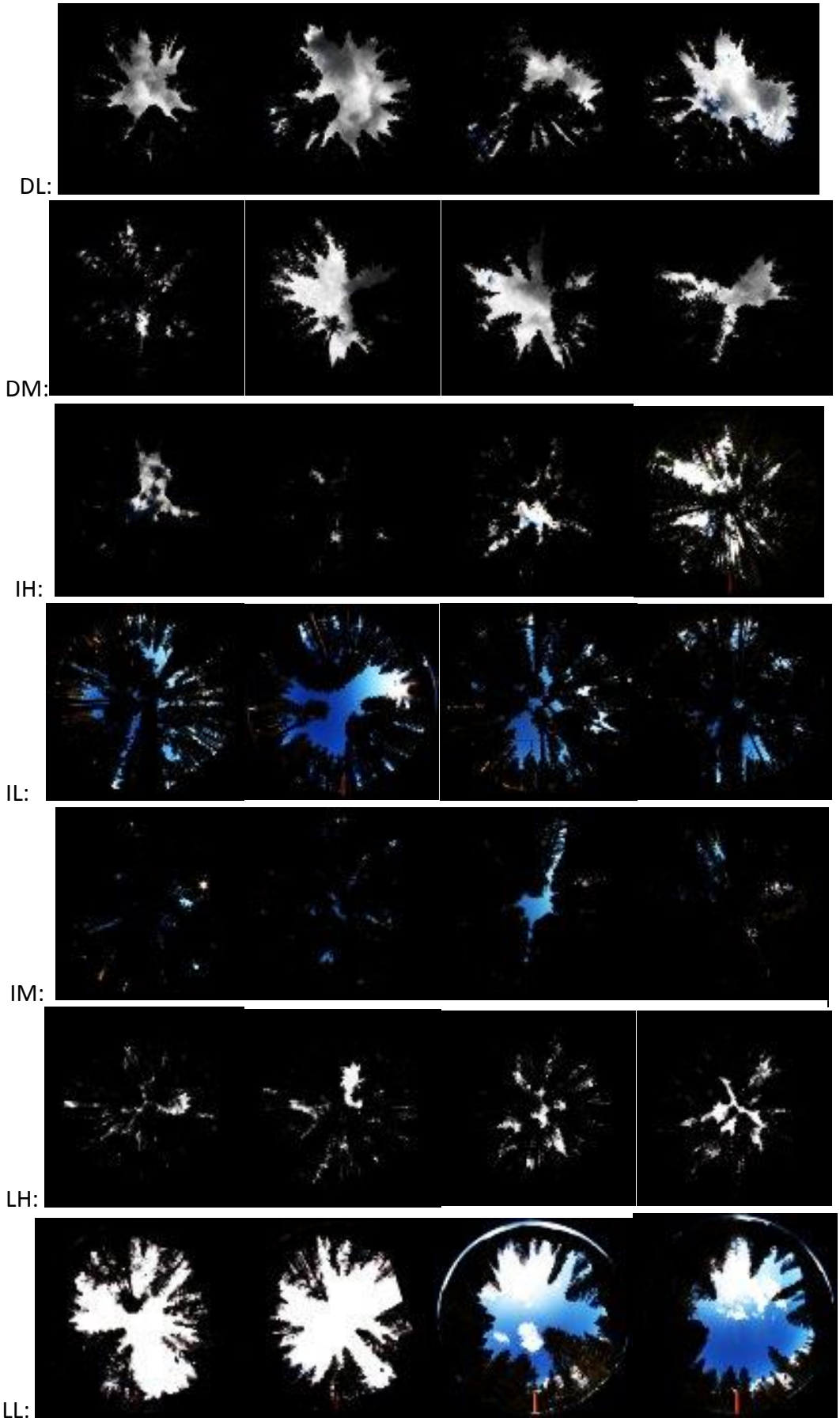

Figure 4.4: B1,C2,D3,E4 HP images in raw format without any color corrections

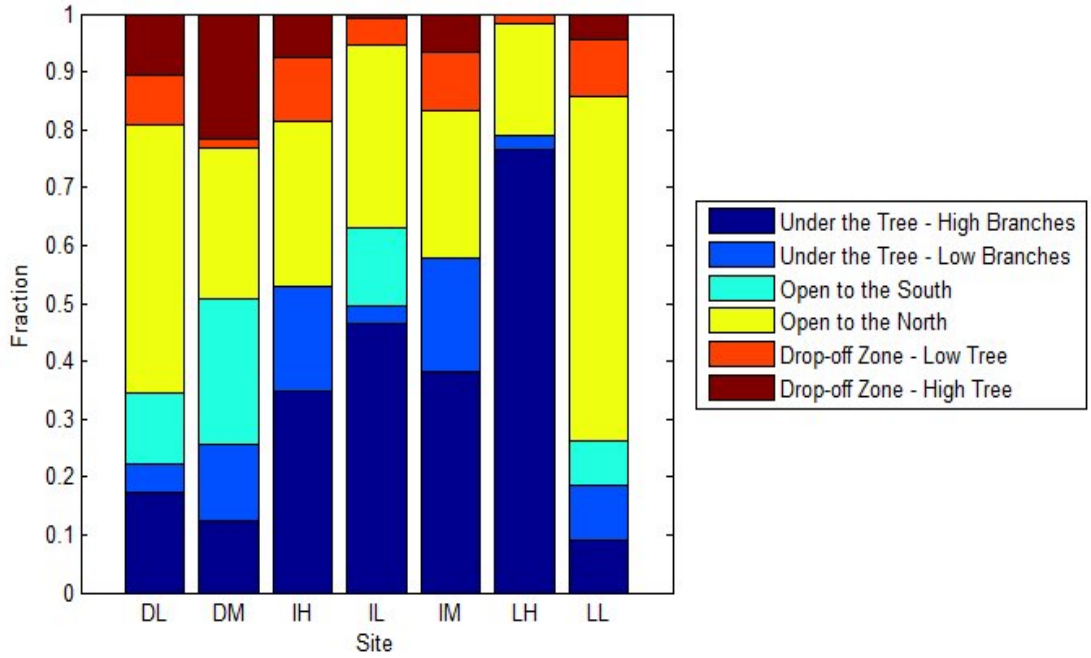

Figure 4.5 Portion of manual canopy categories at each site

Figure 4.5 shows fractions of manual(ly acquired) canopy categories at each site. The fraction of area categorized as under the tree (canopy) varies from 18% at LL to 79% at LH. The denser forest sites, like LH, IH and DM has higher portion of spots under the tree and less partly opened spots. Open to the south category is missing at all in these sites. Dense spruce forests are lack of low branches and the canopy consists mainly of branches high above the ground. Therefore there are not many clear drop-off zones because the intercepted snow is redistributed randomly (and therefore in average more or less uniformly), when it drop-off. Drop-off accumulation requires low branches focusing the snow gliding down to the same spot all the time.

4.4 Snow and canopy categories

The influence of canopy class (from the manual classification) on HS, relative HS and HN is shown in Figures 4.6, 4.7 and 4.8. The analysis reveals that the snow accumulation, ablation and interception depend on canopy category.

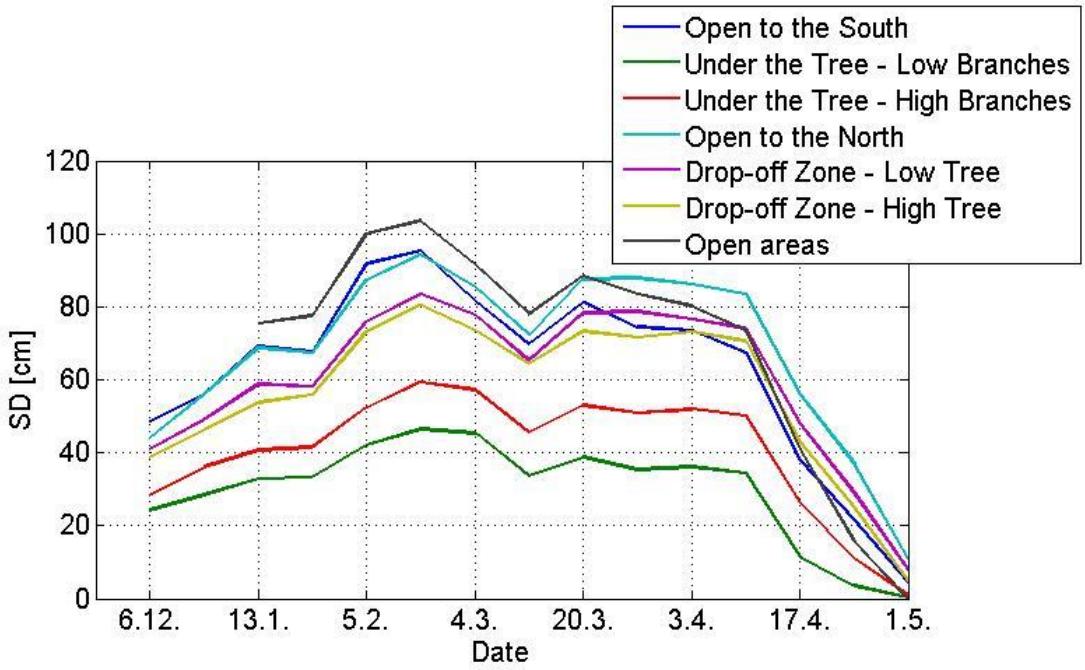

Figure 4.6: Influence of manual canopy classes on snow depth (HS)

Figure 4.6 shows significant differences between HS for places with different canopy structures. During accumulation the highest amount of the snow in the forest was at (partially) open area with no (or low) interception influences during the accumulation period. There is almost no difference between areas open to the north and open to the south. Lower HS occurred in drop-off zones. Lower HS can be explained by compression caused from falling snow. It corresponds with the fact that the HS are lower for drop-off zones of high trees, where the velocity of dropping snow is higher and caused higher compression. As expected, the lowest HS values were observed below the trees due to interception. Higher HS occurred under the trees with higher branches, which are less sheltered against the wind transport of the snow. HS for all classes of forest canopy were lower than for open area during the whole accumulation period. (Relative HS were more or less constant for the accumulation period.)

Interception influence is clearly visible also in Figure 4.7, which shows the amount of new snow for 4 dates after significant snow storms. The lowest HN values were observed under the trees with low branches because of the highest interception. The amount of new snow is higher for spots with more open character, where the interception capacity is lower.

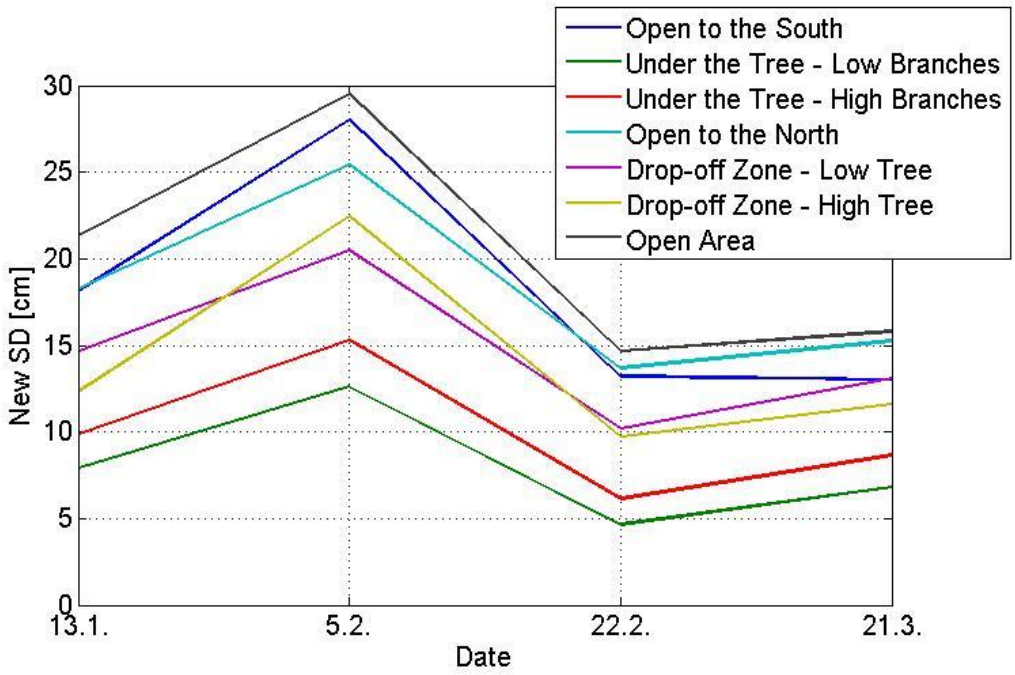

Figure 4.7: Influence of manual canopy classes on new snow depth (total storm depth)

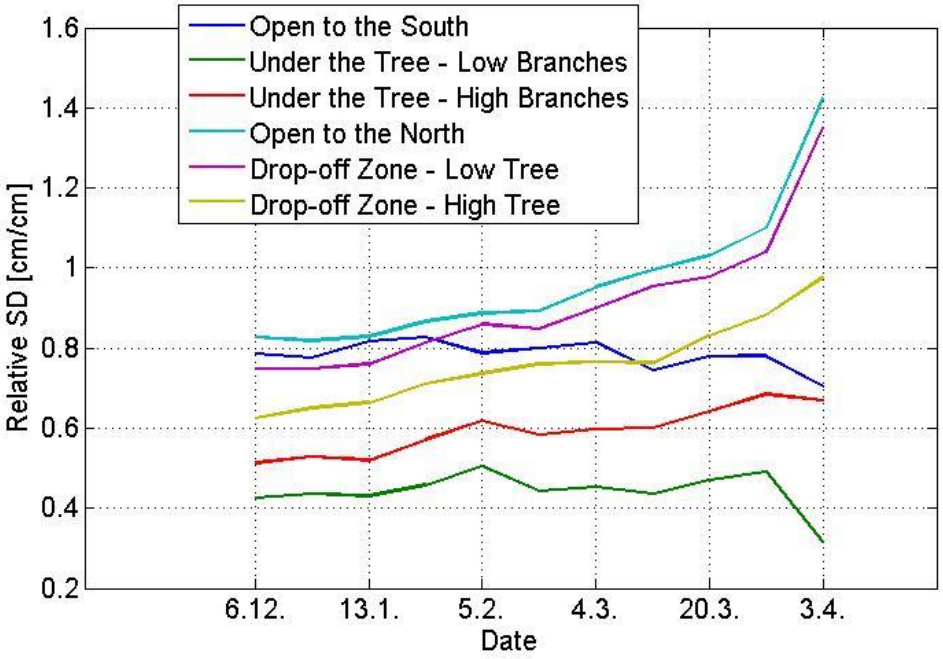

Figure 4.8: Influence of manual canopy classes on relative snow depth (relative to open areas)

The situation greatly changed during the ablation period, when varying HS depletion rates were observed for different canopy classes. This can be better seen in Figure 4.8, which shows HS relative to open areas. Within the Figure 4.8, increasing relative HS corresponds to a lower HS depletion rate as compared to the HS depletion rate in the open. Much lower HS depletion rates were observed for both drop-off zones and for areas open to north. (The HS was higher for these classes than

for the open area at the end of the ablation period.) Also, HS depletion rates for the, 'under tree with high branches class,' was lower than in open areas. UH and ON classes represents areas protected against solar radiation by the canopy. Lower HS depletion rates for drop-off zones could be caused by a higher density of snow compressed by falling snow. The HS depletion rate for open to the south and under low branches was slightly higher than for open areas.

4.5 Canopy characteristics as snow predictors

We were looking for the best snow predictor among the 34 canopy characteristics (metrics) calculated from HP images using the Hemisfer software. Table 4.1 gives an overview of the canopy characteristics. LAI was calculated by pure (Miller 1967) algorithm as well as enhanced by corrections according to Walter et Torquebiau (2000). Gaps metric means the proportion of large gaps estimated according to Chen et Cihlar (1995). For more details about canopy characteristics see section 3.7 above.

Canopy metrics	Entire view	Limited azimuth angle	Limited zenith angle	Combined angle limits
LAI	2	-	-	-
Canopy closure (CCL)	1	4x (S,W,N,E)	2 (0-30°,0-60°)	8
Transmission (TMS)	1	-	3 (0-30°,30-60°,60-90°)	12
Gaps	1	-	-	-

Table 4.1: Overview of canopy metrics analyzed as potential snow predictors

Correlation of the canopy characteristics to relative snow depth (HSr) was studied for 112 points and 15 campaigns. HSr represents relative forest HS to HS at related open area. Using HSr instead of simple HS allows us to better compare the points in distinct time and elevation band. The correlation analysis was split into two parts according to accumulation and ablation period. Table 4.X2 shows an overview of the mean correlation values and their standard deviations for all canopy characteristics. Mean represents absolute value of the mean calculated over all measuring campaigns for each period. Transmission is complementary to CCL. Thus meaning the absolute value of their correlations are equal. Therefore TSM was taken out from the Table 4.2.

The accumulation period exhibits higher correlations with lower standard deviation compared to depletion period. Lower correlation and higher standard deviation for depletion could be caused by snowfall during the beginning of the period. Thus means that not pure depletion processes but also accumulation were in the play, even if the depletion were dominant. There is space for further investigation depletion period, which could be split into mixed sub-period and pure depletion sub-period.

Correlation to relative HS					
Accumulation			Depletion		
Canopy char.	Mean	St.dev.	Canopy char.	Mean	St.dev.
CCL-30	0.80	0.02	CCL-30	0.62	0.12
CCL-60	0.73	0.01	CCL-30W	0.57	0.11
CCL	0.72	0.01	CCL-30E	0.56	0.09
CCL-30S	0.72	0.03	CCL-30N	0.56	0.12
CCL-30W	0.72	0.02	CCL-60	0.53	0.14
Gaps.	0.71	0.01	CCL-30S	0.52	0.12
CCL-90E	0.70	0.02	CCL-90E	0.52	0.13
CCL-60E	0.70	0.02	CCL	0.52	0.14
CCL-60W	0.70	0.02	CCL-60E	0.51	0.13
CCL-30N	0.70	0.02	CCL-60W	0.50	0.12
CCL-30E	0.69	0.02	Gaps.	0.50	0.14
CCL-90W	0.68	0.02	CCL-60N	0.49	0.14
CCL-60N	0.68	0.02	CCL-90N	0.48	0.14
CCL-90N	0.67	0.02	CCL-90W	0.48	0.12
TSM-30-60	0.63	0.01	TSM30-60E	0.43	0.12
CCL-60S	0.62	0.02	TSM-30-60	0.41	0.14
CCL-90S	0.61	0.02	TSM30-60W	0.37	0.09
TSM30-60E	0.58	0.02	CCL-60S	0.36	0.13
LAI-Mi.	0.56	0.02	TSM30-60N	0.36	0.13
LAI-Mi.-cW	0.53	0.01	LAI-Mi.	0.36	0.12
TSM30-60W	0.51	0.01	CCL-90S	0.35	0.13
TSM30-60N	0.50	0.02	LAI-Mi.-cW	0.35	0.12
TSM30-60S	0.49	0.02	TSM60-90N	0.26	0.08
TSM60-90N	0.32	0.02	TSM60-90E	0.25	0.07
TSM60-90E	0.28	0.04	TSM30-60S	0.22	0.13
TSM-60-90	0.28	0.02	TSM-60-90	0.17	0.07
TSM60-90S	0.25	0.01	TSM60-90S	0.12	0.06
TSM60-90W	0.16	0.01	TSM60-90W	0.03	0.06

Table 4.2: Correlation of various canopy characteristic to relative HS for accumulation and depletion period

For the both periods, CCL for 30° view was the best correlated variable (0.80 resp. 0.62) with relative low standard deviation (0.02 res. 0.12). This reflects the high influence of canopy directly above the measured point. The expected higher correlation of south oriented canopy characteristics for depletion was not approved. The LAI had significantly lower correlation to HSr. But at the same time, the LAI is less correlated also to other canopy characteristics, which are almost all highly correlated to each other. The PCA (Figure 4.9) shows that the CCL and the most of the other variables are close to the first component, which explains 97% of data variability. Also according to Stenberg et al. (1999) COP (which is 100% correlated to CCL) does not correlate with LAI. LAI, as additional factor, can increase the predictive power of model. It corresponds to a result of k-means cluster analysis,

which created one large CCL cluster and one tiny cluster consisting only form LAI and Gaps.

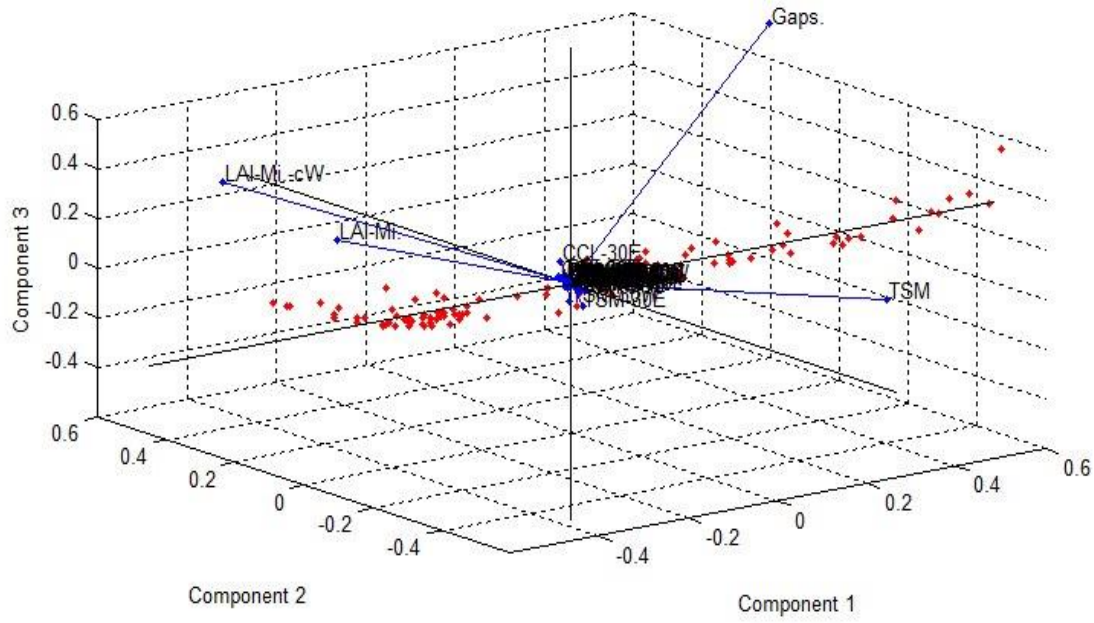

Figure 4.9 PCA clustering of canopy characteristics as potential snow predictors

Huge set of potential snow predictors was reduced to tiny set without loss of predictive power. Never the less the predictive power could be even improved by adding new alternative canopy metrics developed recently by (Moeser 2015). Advantage of the predictor set presented in this study is that it can be completely derived from HP unlike the new metrics requiring extended measurements.

4.6 Snow model

Pure statistical model (SM) and physically based model (PM) for forest snow distribution were utilized as described above in the section 3.13.

SM calculate forest HS (HSf) directly from open area HS (HSo) and the canopy characteristics identified as the best snow predictors in section 4.5 – CCL30 and LAI. (3.13.2-2) and (3.13.2-3) can be rewritten as (4.7.1)

(4.7.1) $HS_f = HS_o * f_{rHS}(CCL30, LAI)$

PM uses mass balance approach estimating interception, drop-off and depletion difference under the canopy. (3.13.3-2)- (3.13.3-6) relations result in (4.7.2)

(4.7.2) $f_{HS} = HS_o - HS_o * f_{IR}(CCL30,LAI) + f_{DO}(DOZ, CCL30, LAI, HS_o) + f_{DD}(CCL30, CCL90S, rHS_o, HS_{fmax})$

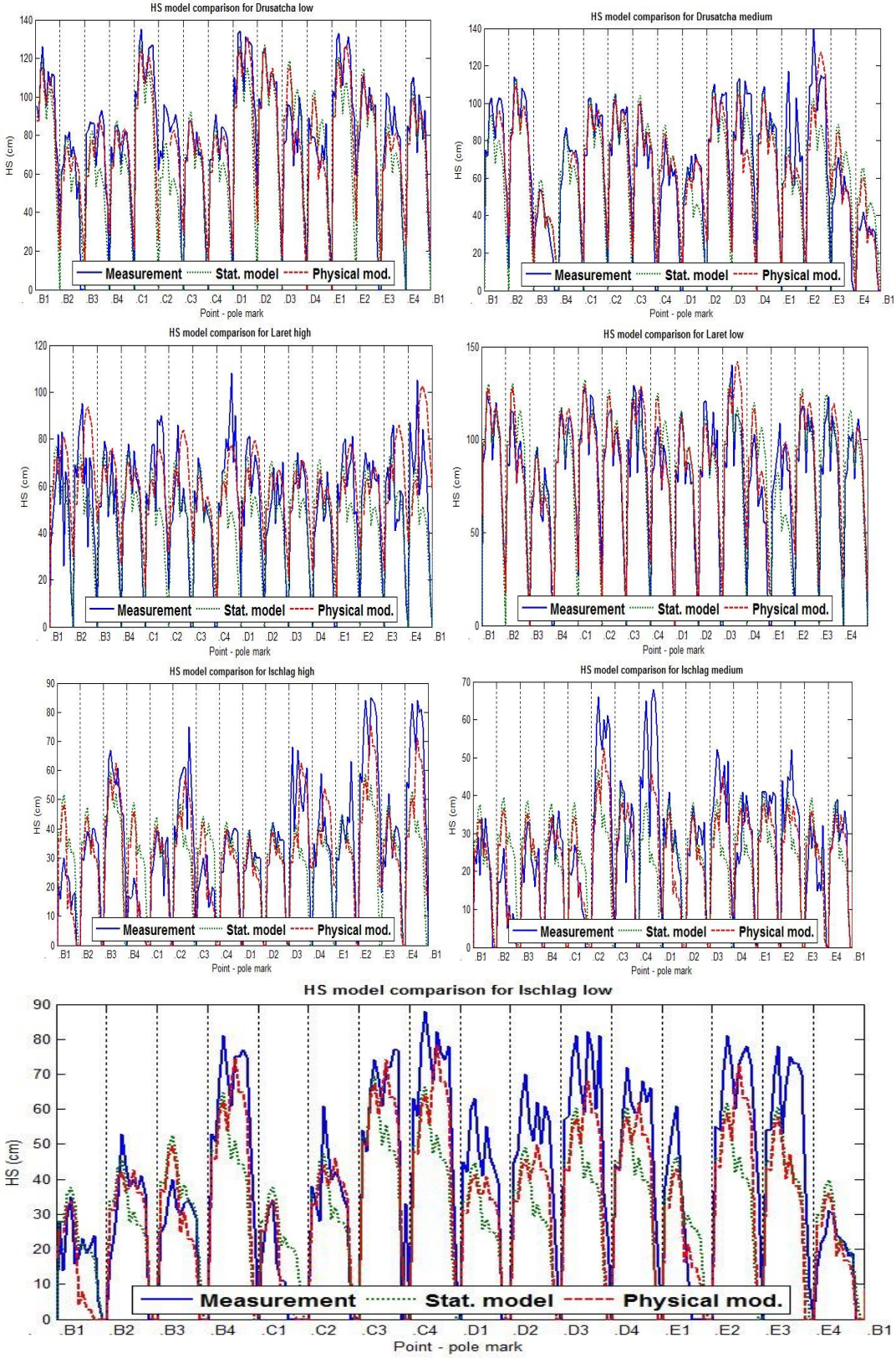

Figure 4.10: Comparison of physical based model to pure statistical model and to observed values.

PM model has the same input requirements as SM extended with delineation of drop-off zones and CCL to south (CCL90S). CCL90S was selected because it reflects canopy openness to the south. Strong influence of direct solar radiation coming from the south direction on depletion was expected. Even if the role of CCL90S was not proved by correlation analysis (see section 4.5), the influence of openness to the south was confirmed in the analysis of manual canopy categorization (see section 4.4). And CCL90S is the variable with the strongest relation to canopy openness to the south from our set of metrics even if its correlation to HS increases only slightly during the depletion. Probably another alternative metrics would explain the canopy openness to the south better then HP based canopy characteristics. Several alternative canopy metrics were recently proposed by Moeser et al. (2015).

Another option to further snow model improvement is taking of potential incoming solar radiation as model parameter. Forests influence snow through the PISR reduction by canopy. The Hemisfer 2 beta version offered new functionality – estimation of PISR under the canopy for specified location and time. Solar radiation measurement was conducted in the frame of this project in order to compare them with Hemisfer 2 beta estimations. We expect that PISR could enhance the snow distribution model mainly for depletion period. . Detailed analysis of gained data is unfortunately out of this study extend. Some results were published in (Moeser et al. 2014).

The model fitness was tested on complete dataset for one season at all sites. Figure 4.10 compares physical model to statistical one and to the observed data. The plots clearly demonstrate that the physical model has better fit to measured data at the most cases. Only very rarely gives the statistical model better result than the physical one. Table 4.3 tells the same story in the words of statistical numbers. Residues and deviation metrics are lower for the PM. Root mean square error (RMSE) is of 15.7 for PM while it is of 13.8 for SM.

	Stochastic Model	**Physical Model**
Residue Sum	16862.816	14251.573
Mean Residue	11.582	10.065
Max. Residue	62.000	59.625
Mean Square Error (MSE)	246.774	190.714
Root Mean Square Error (RMSE)	15.709	13.810
Normalized RMSE [RMSE/(max-min)]	0.112	0.099
Coeff. of Variance [RMSE/mean]	0.290	0.255

Table 4.3: Model comparison

This shows that considering a mass balance approach can enhance the snow distribution model even if very simple mass balance approach is used. The same approach can be applied also for modeling SWE. The SWE model is out of extent of this thesis. Never the less HS values can be used for SWE estimation (Jonas et al. 2009; Sturm et al. 2010; US Army Corps of Engineers 1956)

4.7 Cartesian LiDAR based canopy characteristics – sensitivity analysis

Figure 4.11 shows the correlation between canopy characteristics (LAI and CCL for entire and limited view angle) calculated from hemispherical pictures and the same characteristics derived from LAS (LiDAR) data by Cartesian approach for varying bounding box sizes. The correlations between results from both methods depend on the size of the box around the point taken into account in calculation. Correlations for small boxes are low due to lack of information about canopy above the point in wider zenith view angle. The CCL correlation is better than the LAI correlation and is much less sensitive to box size change.

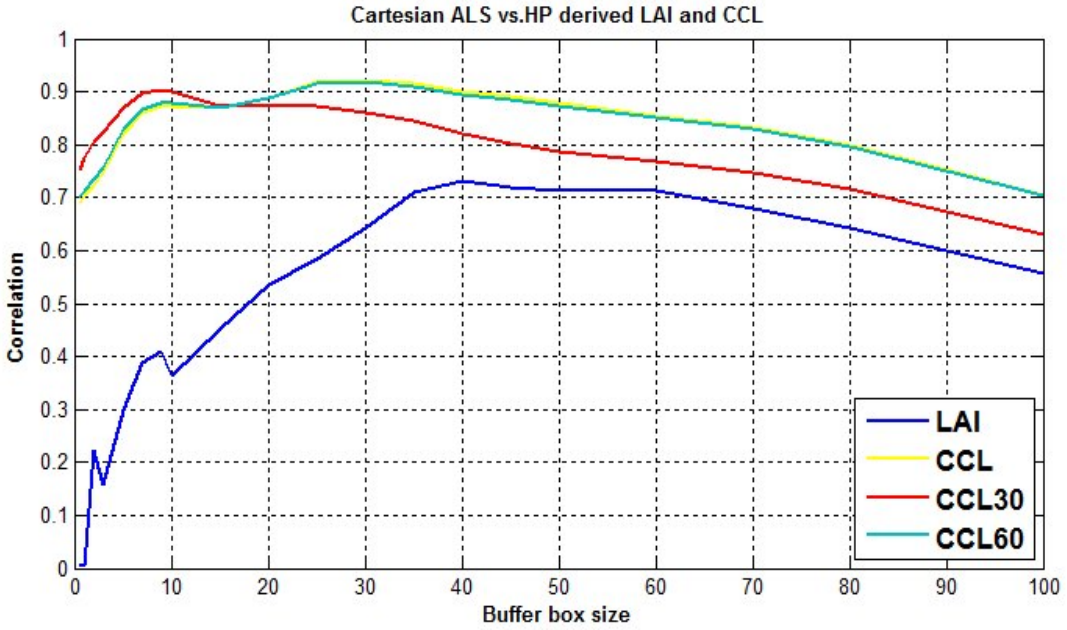

Figure 4.11: Comparison of LiDAR and hemispherical photo derived LAI and CCL for varying bounding box size.

The higher correlation of CCL for limited view angle was expected because of no importance of more distant canopy in this case. That is valid especially for the 30° view. CCL30 correlation is maximal (of 0.90) for only 9m bounding box. But also CCL for entire scope surprisingly starts with quite high correlation for small considered area. It behaves almost identically as CCL60. Dislike the LAI which is scattering and uncorrelated at all for very small buffer counted in. CCL90 and CCL60 correlations reach the maximum (0.92) for the approximately 30m box size. The best match of LAI values was delivered for a 40m box size but the maximal correlation is lower (0.73). After reaching the maximum, all the correlations slowly decrease for the wider considered area, which brings the disrupting extra information into calculations.

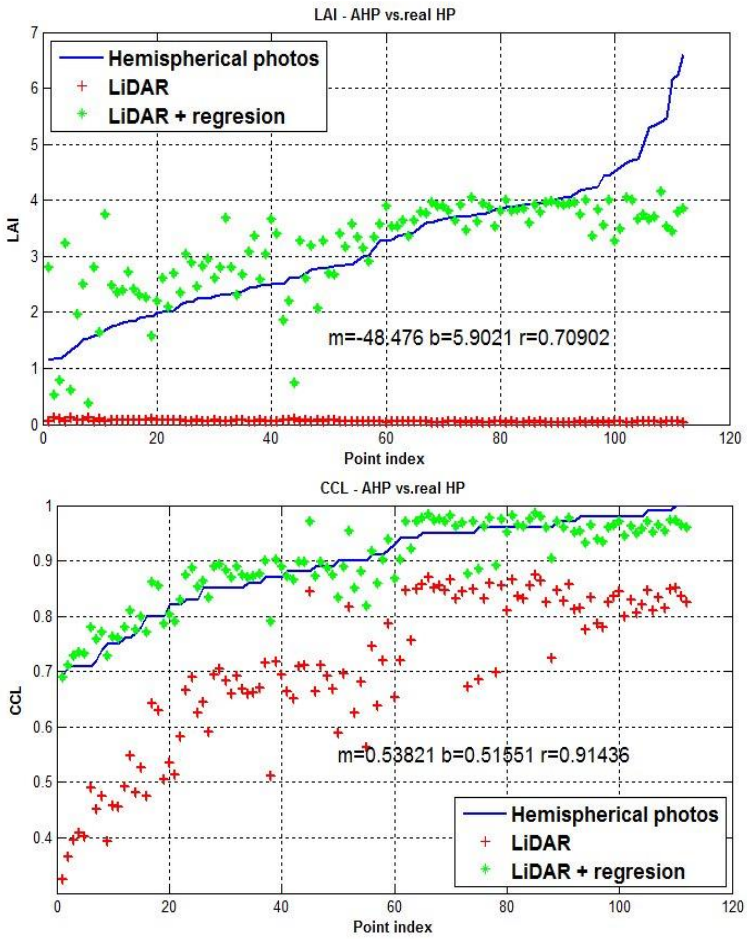

Figure 4.12: Linear transformations applied on Cartesian a/ LAI and b/ CCL and comparison to corresponding HP derived values.

The optimal box size for specific forest site will vary around the above estimated value of 35m depending secondary also on the tree height.

Besides the very good correlation exhibits the Cartesian LiDAR LAI and CCL high normalized root mean square error (NRMSE) of 0.58, resp. 0.66 caused by systematic bias. Figure 4.12 shows linear transformation shifting the LiDAR LAI and CCL values to match the HP based characteristics. Points for each plot were sorted ascending according to real HP based values.

4.8 AHP derived canopy characteristics

The best correlation of AHP derived LAI and CCL to (real) HP was reached for AHP creation algorithm using variable print point size changing linearly from 7 to 0.5 pixel (for image diameter of 700pixels).

AHP derived canopy characteristics correlates to HP based characteristics even better than the Cartesian LiDAR derived values. And more over AHP derived values fit much better to real HP values, without any additional transformation removing the bias, as it is shown in Figure 4.13. The correlation is 0.83 for LAI, respectively 0.92 for CCL. And NRMSE is 0.15 for LAI, respectively 0.12 for CCL. The largest enhancement was achieved for LAI estimation at points with high canopy density, where the Cartesian approach failed.

4.9 Snowpack relation to HP and AHP derived canopy characteristics

The snow depth dependency on canopy closure is captured in Figure 4.14. Figure 4.14a shows HS-CCL relation for selected days during the season: early winter (20th Dec), top accumulation (21st Feb), depletion middle (11th Apr) and the final part of the season (25th Apr). Despite the scatter, there is a decreasing trend in HS with increasing CCL at each time point. Of particular interest is the time of highest accumulation, when the trend is the strongest. Variation of the trends during the entire season is visible in Figure 4.14b. The contour plot gives a complete seasonal overview of HS-CCL relation. These first to plots shows data derived from real HP. The both plots display the increasing reduction of HS with increasing canopy density, which is probably caused by interception.

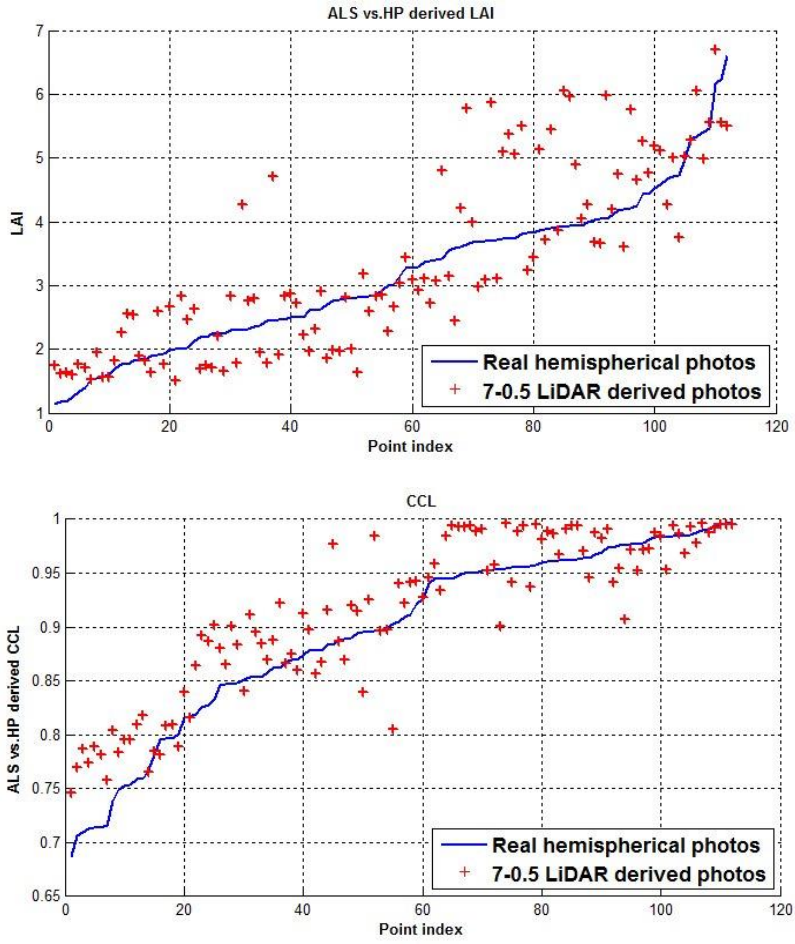

Figure 4.13: Comparison of AHP derived canopy characteristics (LAI and CCL) to corresponding HP derived values.

Comparison of values for the maximum accumulation to values from the mid ablation period (10th April) shows higher differences at points with higher HS, which are mostly the points with lower CCL. The higher HS differences correspond to higher snow depletion rate at spots with lower CCL. Scattering is caused by the fact that HS depends not only on CCL, but also on other factors like drop-off zones and openness to the sun/south.

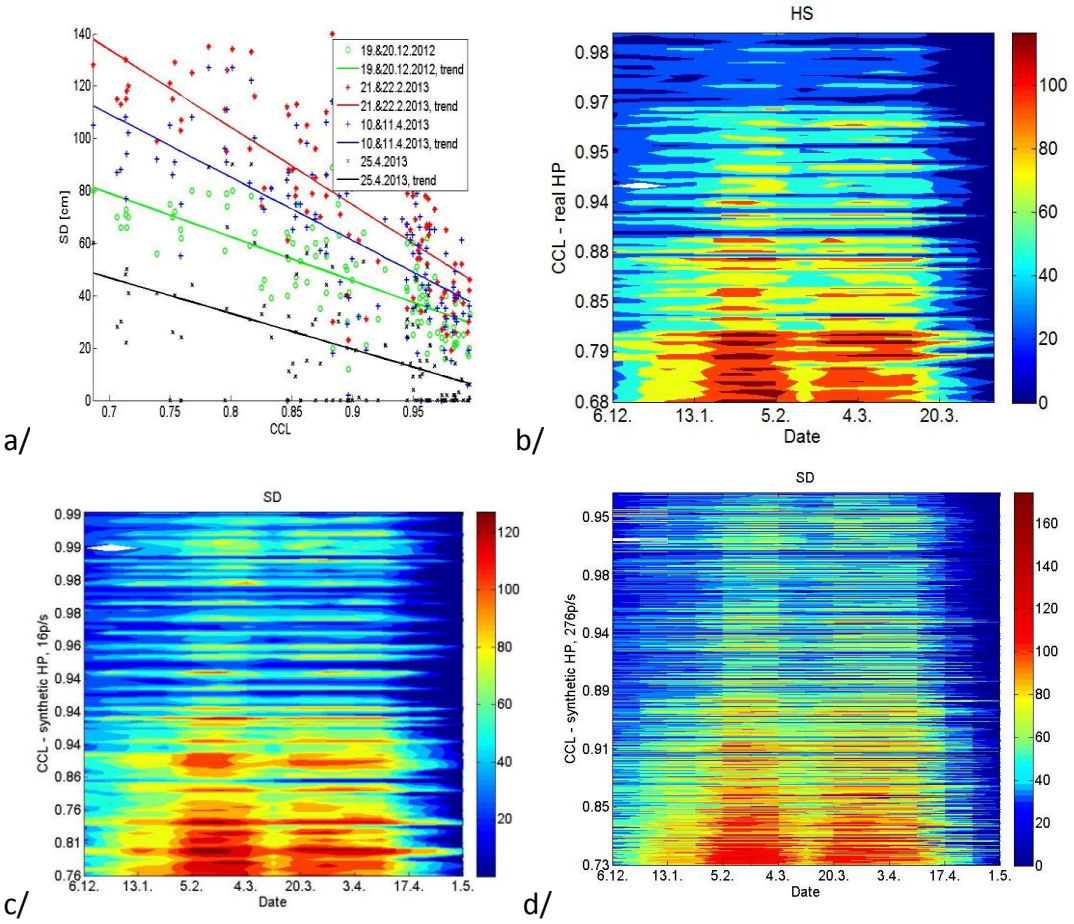

Figure 4.14: The relationship between HS and:
a/ HP derived CCL with highlighted trends for selected campaigns,
b/ HP derived CCL in contour plot for entire season,
c/ AHP derived CCL,
d/ AHP derived CCL for larger point set (276 points per site)

Figure 4.14 c/ and d/ shows the same HS-CCL-time contour plot gained from AHP instead of real HP. Plot c/ is created for the same point set as previous plot for real HP CCL. It shows the same patterns in spatial-temporal distribution of HS. We were not able to take real HP for all 7x276 points at the sites, because it was too time consumptive. But the AHP for this huge complete point set was generated much easier and faster. The plot d/ shows the HS-CCL relation for this entire point set. The same patterns could be found in all of the plots. This case demonstrates the applicability of AHP for large or inaccessible areas.

Snow-HP canopy characteristics relation is discussed also in section 4.6 Snow model, where real HP derived values were used as input parameters. Good correspondence of AHP to RHP and ability to use AHP instead RHP enhance the applicability of the model for much larger areas.

5. Conclusions

Spatial and temporal distribution of snow in forests is driven by canopy structure which impacts radiation conditions, heat and material fluxes. The results show that there is significant correlation between canopy metrics and snow characteristics in small scale. There is a difference between the impact of canopy on accumulation and on depletion processes. As expected, lower HS values were observed beneath the denser canopy during the accumulation period. The situation turned around during the ablation period, when: 1) lower HS depletion rates in denser forest held snow longer compared to open areas and 2) aspect of the canopy gaps came into play.

The canopy closure for 30° zenith angle was considered as the best HS predictor among the 34 investigated canopy characteristics, because it has the highest correlation to HS (correlation coefficient of 0.8 for accumulation period and 0.62 for depletion period).

The CCL30 together with the LAI and CCLS was taken as the input parameters for snow model. The comparison of pure stochastic model to the physical based model considering mass balance shows that mass balance calculations considering interception, drop-off and depletion rate difference can enhance the predictive power of the snow distribution model.

There is a potential of further model improvement by incorporating more complex mass balance equations or by finding an even better alternative snow predictor – the good candidate could be potential incoming solar radiation (PISR), which can be derived from HP images by the new version of Hemisfer software.

Simple manual canopy categorization was proposed as an alternative to standard canopy metrics. It allows quick canopy assessment without any technical equipment. The categories were tailored to reflect the canopy properties influencing snow pack. Therefore it was able to confirm the expected impact of canopy openness aspect. Southwards oriented openings demonstrate higher depletion rates. Dislike the standard canopy metrics, manual canopy categorization allows to identify the drop-off zones. Disadvantage of the method is less exactness compared to standard canopy metrics, even if the results show a favorable correlation between assessments from distinct observers. Although it is much less time consuming than HP, its applicability for very large areas is still limited.

The standard canopy metrics can be obtained by several methods. Each method offers some advantages. (Real) HP is a standard method, which is proved by the long usage history, and which returns reliable results. However it requires a lot of field work and data processing, limiting the HP applicability in a large area, inaccessible spots or high resolution surveys, unlike ALS/aerial LiDAR. The correlation of CCL resp. LAI derived from LiDAR data using the Cartesian approach to reference HP CCL resp. LAI was 0.93 resp. 0.72 for the 30m resp. 40m considered buffer. The LAI estimation was significantly biased for the high LAI values. Artificial HP created by algorithm varying the point print size 0.5-7 pixels gives an even better

correlation of CCL resp. LAI (0.93 resp. 0.83) and lower bias in whole canopy density range. LiDAR data requires more complicated processing than HP images. The data processing can be automatized unlike the HP fieldwork. We can conclude that aerial LiDAR data can be successfully used instead of hemispherical photography.

Figure 5.1: Variable forest environment causes snow cover variations

6. References

Anderson, M.C. 1971. Radiation and crop structure. Plant Photosynth. Prod. Man. methods. Hague, Netherlands Junk 412–466.

Anderson, M.C. 1964. Studies of the Woodland Light Climate: I. The Photographic Computation of Light Conditions. J. Ecol. 52, 27–41.

Armstrong, R.L., Brun, E. 2008. Snow and Climate: Physical Processes, Surface Energy Exchange and Modeling. Cambridge University Press.

Bauhahn, P.E., Fritz, B.S., Krafthefer, B.C. 2009. Systems and methods for safe laser imaging, detection and ranging (lidar) operation.

Bonhomme, R., Varlet-Grancher, C., Chartier, M. 1974. The use of hemispherical photographs for determining the leaf area index of young crops. Photosynthetica 8, 299–301.

Brack, C.L. 2000. Forest Inventory - Measuring a Forest [WWW Document]. Comput. course Resour. For. Invent. Aust. Natl. Univ. URL http://fennerschool-associated.anu.edu.au/mensuration/forest.htm

Brack, C.L. 1999. Forest Measurement and Modeling - Measuring trees, stands and forests for effective forest management [WWW Document]. Comput. course Resour. For. Meas. Model. Aust. Natl. Univ. URL http://fennerschool-associated.anu.edu.au/mensuration/home.htm

Brändli, U.-B., Ciodi, F., Fischer, C., Huber, M. 2015. Swiss National Forest Inventory – Special assessments for the Forest Report 2015. Birmensdorf.

Brown, R.D., Mote, P.W. 2009. The Response of Northern Hemisphere Snow Cover to a Changing Climate*. J. Clim. 22, 2124–2145. doi:10.1175/2008JCLI2665.1

Carlson, T.N., Ripley, D.A. 1997. On the relation between NDVI, fractional vegetation cover, and leaf area index. Remote Sens. Environ. 62, 241–252. doi:10.1016/S0034-4257(97)00104-1

Colbeck, S., Akitaya, E., Armstrong, R., Gubler, H., Lafeuille, J., Lied, K., McClung, D., Morris, E. 1990. The International Classification for Seasonal Snow on the Ground.

Cornelius, J.P., Wightman, K.E., Grogan, J.E., Ward, S.E. 2004. Encyclopedia of Forest Sciences. Encycl. For. Sci. doi:10.1016/B0-12-145160-7/00190-3

Da Silva, D., Balandier, P., Boudon, F., Marquier, A., Godin, C. 2011. Modeling of light transmission under heterogeneous forest canopy: an appraisal of the effect of the precision level of crown description. Ann. For. Sci. 69, 181–193. doi:10.1007/s13595-011-0139-2

Deems, J.S., Painter, T.H., Finnegan, D.C. 2013. Lidar measurement of snow depth: a review. J. Glaciol. 59, 467–479. doi:10.3189/2013JoG12J154

Dietz, A.J., Kuenzer, C., Gessner, U., Dech, S. 2012. Remote sensing of snow – a review of available methods. Int. J. Remote Sens. 33, 4094–4134. doi:10.1080/01431161.2011.640964

Dingman, S.L. 2002. Physical hydrology. doi:10.1177/030913338901300106

EEA-European Environment Agency 2015a. The European environment — state and outlook 2015: synthesis report. Copenhagen. doi:10.2800/944899

EEA-European Environment Agency 2015b. Water-retention potential of Europe's forests. EEA Tech. Rep. 13/2015. doi:10.2800/790618

FAO 2015. Global Forest Resources Assessment 2015. Rome.

Fierz, C.; Armstrong, R.L.; Durand, Y.; Etchevers, P.; Greene, E.; McClung, D.M.; Nishimura, K.; Satyawali, P.K.; Sokratov, S.A. 2009. The International Classification of Seasonal Snow on the Ground, in: IHP-VII Technical Documents in Hydrology No 83, IACS Contribution No 1. Paris, UNESCO-IHP. 80 S.

FOEN - Federal Office for the Environment 2015. Forest and Wood in Switzerland [WWW Document]. URL www.bafu.admin.ch/ud-1093-e

Frazer, G.W., Canham, C.D., Lertzman, K.P. 1999. Gap Light Analyzer (GLA), Version 2.0: Imaging software to extract canopy structure and gap light transmission indices from true-colour fisheye photographs, users manual and program documentation. Simon Fraser Univ. Burn. Br. Columbia, Inst. Ecosyst. Stud. Millbrook, New York 36.

Gladt, M., Bednar, T. 2013. A new method for the calculation of the sky view factor for non-rectangular surroundings, in: Proceedings of BS 2013: 13th Conference of the International Building Performance Simulation Association. pp. 2839–2844.

Gonsamo, A., D'odorico, P., Pellikka, P. 2013. Measuring fractional forest canopy element cover and openness - definitions and methodologies revisited. Oikos 122, 1283–1291. doi:10.1111/j.1600-0706.2013.00369.x

Güntner, A., Stuck, J., Werth, S., Döll, P., Verzano, K., Merz, B. 2007. A global analysis of temporal and spatial variations in continental water storage. Water Resour. Res. 43, n/a–n/a. doi:10.1029/2006WR005247

Haboudane, D. 2004. Hyperspectral vegetation indices and novel algorithms for predicting green LAI of crop canopies: Modeling and validation in the context of precision agriculture. Remote Sens. Environ. 90, 337–352. doi:10.1016/j.rse.2003.12.013

Hall, D.K., Martinec, J. 2012. Remote Sensing of Ice and Snow. Springer Science & Business Media.

Ham, R.D. 1982. FOG DRIP IN THE BULL RUN MUNICIPAL WATERSHED, OREGON1. JAWRA J. Am. Water Resour. Assoc. 18, 785–789. doi:10.1111/j.1752-1688.1982.tb00073.x

Helfricht, K., Schöber, J., Seiser, B., Fischer, A., Stötter, J., Kuhn, M. 2012. Snow accumulation of a high alpine catchment derived from LiDAR measurements. Adv. Geosci. 32, 31–39. doi:10.5194/adgeo-32-31-2012

Hill, R. 1924. A lens for whole sky photographs. Q. J. R. Meteorol. Soc. 50, 227–235. doi:10.1002/qj.49705021110

Hobbs, P. V 2010. Ice Physics, Oxford Classic Texts in the Physical Sciences. OUP Oxford.

Chang, M. 2012. Forest Hydrology: An Introduction to Water and Forests. CRC Press.

Chen, J.M., Cihlar, J. 1995. Quantifying the effect of canopy architecture on optical measurements of leaf area index using two gap size analysis methods. IEEE Trans. Geosci. Remote Sens. 33, 777–787. doi:10.1109/36.387593

Chianucci, F., Cutini, A. 2012. Digital hemispherical photography for estimating forest canopy properties: current controversies and opportunities. iForest - Biogeosciences For. 5, 290–295. doi:10.3832/ifor0775-005

Jennings, S. 1999. Assessing forest canopies and understorey illumination: canopy closure, canopy cover and other measures. Forestry 72, 59–74. doi:10.1093/forestry/72.1.59

Jonas, T., Essery, R. 2011. Snow cover and snowmelt in forest regions, in: Singh, V.P., Haritashya, U.K. (Eds.), Encyclopedia of Snow, Ice and Glaciers. Springer, Dordrecht, Heidelberg, pp. 1033–1036.

Jonas, T., Marty, C., Magnusson, J. 2009. Estimating the snow water equivalent from snow depth measurements in the Swiss Alps. J. Hydrol. 378, 161–167. doi:10.1016/j.jhydrol.2009.09.021

Jonckheere, I., Fleck, S., Nackaerts, K., Muys, B., Coppin, P., Weiss, M., Baret, F. 2004. Review of methods for in situ leaf area index determination. Agric. For. Meteorol. 121 19–35. doi:10.1016/j.agrformet.2003.08.027

Jonckheere, I., Nackaerts, K., Muys, B., Coppin, P. 2005. Assessment of automatic gap fraction estimation of forests from digital hemispherical photography. Agric. For. Meteorol. 132, 96–114. doi:10.1016/j.agrformet.2005.06.003

Korhonen, L., Korpela, I., Heiskanen, J., Maltamo, M. 2011. Airborne discrete-return LIDAR data in the estimation of vertical canopy cover, angular canopy closure

and leaf area index. Remote Sens. Environ. 115, 1065–1080. doi:10.1016/j.rse.2010.12.011

Kukko, A., Anttila, K., Manninen, T., Kaasalainen, S., Kaartinen, H. 2013. Snow surface roughness from mobile laser scanning data. Cold Reg. Sci. Technol. 96, 23–35. doi:10.1016/j.coldregions.2013.09.001

Lang, A., Xiang 1986. Estimation of leaf area index from transmission of direct sunlight in discontinuous canopies. Agric. For. Meteorol. 37, 229–243. doi:10.1016/0168-1923(86)90033-X

Lang, A.R.G. 1987. Simplified estimate of leaf area index from transmittance of the sun's beam. Agric. For. Meteorol. 41, 179–186. doi:10.1016/0168-1923(87)90078-5

Leblanc, S.G., Chen, J.M., Fernandes, R., Deering, D.W., Conley, A. 2005. Methodology comparison for canopy structure parameters extraction from digital hemispherical photography in boreal forests. Agric. For. Meteorol. 129, 187–207. doi:10.1016/j.agrformet.2004.09.006

Lehning, M., Bartelt, P., Brown, B., Fierz, C., Satyawali, P. 2002. A physical SNOWPACK model for the Swiss avalanche warning Part II: Snow microstructure. COLD Reg. Sci. Technol. 35, 147–167. doi:10.1016/S0165-232X(02)00073-3

LI-COR Inc. 1992. LAI-2000 Plant Canopy Analyzer Instruction/Operating Manual.

Lieffers, V.J., Messier, C., Stadt, K.J., Gendron, F., Comeau, P.G. 1999. Predicting and managing light in the understory of boreal forests. Can. J. For. Res.

Lugo, A.E., Brown, S.L., Dodson, R., Smith, T.S., Shugart, H.H. 1999. The Holdridge life zones of the conterminous United States in relation to ecosystem mapping. J. Biogeogr. 26, 1025–1038. doi:10.1046/j.1365-2699.1999.00329.x

McClung, D., Schaerer, P.A. 2006. The Avalanche Handbook, Mountaineers Bks. Mountaineers Books.

Miller, J.B. 1967. A formula for average foliage density. Aust. J. Bot. 15, 141–144.

Moeser, D., Morsdorf, F., Jonas, T. 2015. Novel forest structure metrics from airborne LiDAR data for improved snow interception estimation. Agric. For. Meteorol. 208, 40–49. doi:10.1016/j.agrformet.2015.04.013

Moeser, D., Roubinek, J., Schleppi, P., Morsdorf, F., Jonas, T. 2014. Canopy closure, LAI and radiation transfer from airborne LiDAR synthetic images. Agric. For. Meteorol. 197, 158–168. doi:10.1016/j.agrformet.2014.06.008

Monsi, M., Saeki, T. 1953. Über den Lichtfaktor in den Pflanzengesellschaften und seine Bedeutung für die Stoffproduktion. Japanese J. Bot. 14, 22–52.

Morsdorf, F., Kötz, B., Meier, E., Itten, K.I., Allgöwer, B. 2006. Estimation of LAI and fractional cover from small footprint airborne laser scanning data based on gap fraction. Remote Sens. Environ. 104, 50–61. doi:10.1016/j.rse.2006.04.019

Munter, W. 2014. 3x3 Lawinen: Risikomanagement im Wintersport. Tappeiner AG.

Myneni, R.B., Ross, J., Asrar, G. 1989. A review on the theory of photon transport in leaf canopies. Agric. For. Meteorol. 45, 1–153. doi:10.1016/0168-1923(89)90002-6

Nilson, T. 1971. A theoretical analysis of the frequency of gaps in plant stands. Agric. Meteorol. 8, 25–38. doi:10.1016/0002-1571(71)90092-6

NOAA-NGS 2015. Light Detection and Ranging (LIDAR) [WWW Document]. Natl. Ocean. Atmos. Adm. - Natl. Geod. Surv. URL http://www.ngs.noaa.gov/RESEARCH/RSD/main/lidar/lidar.shtml (accessed 5.20.15).

Norman J.M., C.G.S. 1989. Canopy strcture, in: Pearcy R.W., Ehleringer J.R., Mooney H.A., R.P.W. (Ed.), Plant Physiological Ecology: Field Methods and Instrumentation. Chapman and Hall, New York, pp. 301–325.

Parent, J.R., Volin, J.C. 2014. Assessing the potential for leaf-off LiDAR data to model canopy closure in temperate deciduous forests. ISPRS J. Photogramm. Remote Sens. 95, 134–145. doi:10.1016/j.isprsjprs.2014.06.009

Pukkala, T., Kuuluvainen, T., Stenberg, P. 1993. Below-canopy distribution of photosynthetically active radiation and its relation to seedling growth in a boreal Pinus sylvestris stand: a simulation approach. Scand. J. For. Res.

Revuelto, J., López-Moreno, J.I., Azorin-Molina, C., Zabalza, J., Arguedas, G., Vicente-Serrano, S.M. 2014. Mapping the annual evolution of snow depth in a small catchment in the Pyrenees using the long-range terrestrial laser scanning. J. Maps 10, 379–393. doi:10.1080/17445647.2013.869268

Richards, J.A. 2013. Remote Sensing Digital Image Analysis, Remote Sensing Digital Image Analysis: An Introduction. Springer Berlin Heidelberg, Berlin, Heidelberg. doi:10.1007/978-3-642-30062-2

Rosegrant, M.W., Cai, X., Cline, S.A. 2002. Global water outlook to 2025, in: A 2020 Vision for Food Agriculture and the Environment. International Food Policy Research Institute, Washington, DC, USA.

Rutter, N., Essery, R., Pomeroy, J., Altimir, N., Andreadis, K., Baker, I., Barr, A., Bartlett, P., Boone, A., Deng, H., Douville, H., Dutra, E., Elder, K., Ellis, C., Feng, X., Gelfan, A., Goodbody, A., Gusev, Y., Gustafsson, D., Hellstroem, R., Hirabayashi, Y., Hirota, T., Jonas, T., Koren, V., Kuragina, A., Lettenmaier, D., Li, W.-P., Luce, C., Martin, E., Nasonova, O., Pumpanen, J., Pyles, R.D., Samuelsson, P., Sandells, M., Schaedler, G., Shmakin, A., Smirnova, T.G., Staehli, M., Stoeckli, R., Strasser, U., Su, H., Suzuki, K., Takata, K., Tanaka,

K., Thompson, E., Vesala, T., Viterbo, P., Wiltshire, A., Xia, K., Xue, Y., Yamazaki, T. 2009. Evaluation of forest snow processes models (SnowMIP2). J. Geophys. Res. 114. doi:10.1029/2008JD011063

Ryu, Y., Sonnentag, O., Nilson, T., Vargas, R., Kobayashi, H., Wenk, R., Baldocchi, D.D. 2010. How to quantify tree leaf area index in an open savanna ecosystem: A multi-instrument and multi-model approach. Agric. For. Meteorol. 150, 63–76. doi:10.1016/j.agrformet.2009.08.007

Seidl, K., Martinec, J. 2004. Remote sensing in Snow Hydrology.

Schaer, P. 2010. In-flight Quality Assessment and Data Processing for Airborne Laser Scanning. Geodätisch-geophysikalische Arb. der Schweiz 79.

Schleppi, P., Conedera, M., Sedivy, I., Thimonier, A. 2007. Correcting non-linearity and slope effects in the estimation of the leaf area index of forests from hemispherical photographs. Agric. For. Meteorol. 144, 236–242. doi:10.1016/j.agrformet.2007.02.004

Schowengerdt, R.A. 2012. Remote sensing: Models and methods for image processing: Second edition, Remote Sensing: Models and Methods for Image Processing: Second Edition. Elsevier Inc.

Singh, P., Singh, V. 2001. Snow and Glacier Hydrology, Water Science and Technology Library. Springer Netherlands, London.

Solberg, S., Brunner, A., Hanssen, K.H., Lange, H., Næsset, E., Rautiainen, M., Stenberg, P. 2009. Mapping LAI in a Norway spruce forest using airborne laser scanning. Remote Sens. Environ. 113, 2317–2327. doi:10.1016/j.rse.2009.06.010

Sprugel, D.G., Brooks, J.R., Hinckley, T.M. 1996. Effects of light on shoot geometry and needle morphology in Abies amabilis. Tree Physiol. 16, 91–98.

Stenberg, P., Kangas, T., Smolander, H., Linder, S. 1999. Shoot structure, canopy openness, and light interception in Norway spruce. Plant. Cell Environ. 22, 1133–1142. doi:10.1046/j.1365-3040.1999.00484.x

Storck, P., Lettenmaier, D.P., Bolton, S.M. 2002. Measurement of snow interception and canopy effects on snow accumulation and melt in a mountainous maritime climate, Oregon, United States. Water Resour. Res. 38, 51–516.

Sturm, M., Taras, B., Liston, G.E., Derksen, C., Jonas, T., Lea, J. 2010. Estimating Snow Water Equivalent Using Snow Depth Data and Climate Classes. J. Hydrometeorol. 11, 1380–1394. doi:10.1175/2010JHM1202.1

SwissTopo 2013. DOM [WWW Document]. URL http://www.swisstopo.admin.ch/internet/swisstopo/en/home/products/height/dom_dtm-av.html (accessed 9.9.13).

Thimonier, A., Sedivy, I., Schleppi, P. 2010. Estimating leaf area index in different types of mature forest stands in Switzerland: a comparison of methods. Eur. J. For. Res. 129, 543–562. doi:10.1007/s10342-009-0353-8

TopoSys 2015. TopoSys Lidar Solutions [WWW Document]. URL http://www.imagemaps.com/toposys.htm (accessed 7.7.15).

Tupin, F., Inglada, J., Nicolas, J.M. 2014. Remote Sensing Imagery, Remote Sensing Imagery. John Wiley & Sons, Inc., Hoboken, USA. doi:10.1002/9781118899106

US Army Corps of Engineers 1956. No Title. North Pacific Division, Corps of Engineers, U.S. Army, Portland.

Walter, J.-M.N., Torquebiau, E.F. 2000. The computation of forest leaf area index on slope using fish-eye sensors. Comptes Rendus l'Académie des Sci. - Ser. III - Sci. la Vie 323, 801–813. doi:10.1016/S0764-4469(00)01229-4

Wang, Y., Woodcock, C.E., Buermann, W., Stenberg, P., Voipio, P., Smolander, H., Häme, T., Tian, Y., Hu, J., Knyazikhin, Y., Myneni, R.B. 2004. Evaluation of the MODIS LAI algorithm at a coniferous forest site in Finland. Remote Sens. Environ. 91, 114–127. doi:10.1016/j.rse.2004.02.007

Waring, R.H. 2002. Temperate coniferous forests, in: Mooney, H., Canadell, J. (Eds.), Encyclopedia of Global Environmental Change. John Wiley and Sons Ltd, London, pp. 560–565.

Waring, R.H., Running, S.W. 1978. Sapwood Water Storage: its Contribution to Transpiration and Effect Upon Water Con- ductance Through the Stems of Old-growth Douglas-fir. Plant. Cell Environ. 1, 131–140.

Webb, N. (ed. . 1999. Hemiview User Manual [WWW Document]. URL ftp://ftp.dynamax.com/manuals/HemiView_Manual.pdf

Weiss, M., Baret, F., Smith, G.J., Jonckheere, I., Coppin, P. 2004. Review of methods for in situ leaf area index (LAI) determination. Agric. For. Meteorol. 121, 37–53. doi:10.1016/j.agrformet.2003.08.001

WSL 2007. Erste Ergebnisse des dritten Landesforstinventars LFI3. Birmensdorf.

Figure source references

Canadian Avalanche Association, 2015. Canadian Avalanche Association [WWW Document]. URL http://www.avalancheassociation.ca/ (accessed 10.11.15).

Kalma, D., 2015. denniskalma.com [WWW Document]. URL http://www.denniskalma.com/ (accessed 10.11.15).

kurtz-fernhout.com, 2015. kurtz-fernhout.com [WWW Document]. URL http://kurtz-fernhout.com/ (accessed 10.11.15).

Libbrecht, K.G., 2015. SnowCrystals.com [WWW Document]. URL http://www.snowcrystals.com/ (accessed 10.11.15).

NASA, 2015. Land Data Assimilation System (LDAS) [WWW Document]. URL http://ldas.gsfc.nasa.gov/ (accessed 10.11.15).

NOAA, 2015. National Oceanic and Atmospheric Administration, US Department of Commerce [WWW Document]. URL http://www.noaa.gov/

NSIDC, 2015. National Snow and Ice Data Center [WWW Document]. URL http://nsidc.org/ (accessed 10.11.15).

Smith, C., 2015. The Naked Scientists [WWW Document]. URL http://www.thenakedscientists.com/

WeatherBELL Analytics, 2015. WeatherBELL Analytics [WWW Document]. URL http://www.weatherbell.com/

WSL, 2015. Swiss National Forest Inventory [WWW Document]. URL http://www.lfi.ch

7. Acknowledgement

Thanks to the mountains that they bear snow, thanks to snow for guarding the mountains. Thanks God or nature for gifting me with the passion for snow and mountains.

Further thanks to all the people sharing this passion with me. Special thanks to all who helped me to learn more about snow and nature. There is not enough space for all the names, let me mention a few of them: Tobias Jonas, David Moeser and all nice people I met at SLF; Jiří Pavlásek and Michal Jeníček from tiny Czech snow science community; Thomas Wiesinger and colleagues from Mountain risk engineering and Mountain forestry department of BOKU university in Vienna .

Also because the living in Switzerland is not for free, thanks for the foundation from the ERASMUS internship program, WSL Institute for Snow and Avalanche Research SLF and Czech University of Life Sciences in Prague.